UNIVERSITY OF CAMPINAS

School of Chemical Engineering

VICTOR DE BACKER MOURA

STUDY OF FLUIDIZATION REGIMES BY SHANNON ENTROPY

ESTUDO SOBRE REGIMES DE FLUIDIZAÇÃO VIA ENTROPIA DE SHANNON

CAMPINAS

2018

VICTOR DE BACKER MOURA

STUDY OF FLUIDIZATION REGIMES BY SHANNON ENTROPY

ESTUDO SOBRE REGIMES DE FLUIDIZAÇÃO VIA ENTROPIA DE SHANNON

Supervisor: Prof. Dr. Marco Aurélio Cremasco

Dissertação apresentada à Faculdade de Engenharia Química da Universidade Estadual de Campinascomo parte dos requisitos necessários para a obtenção do título de Mestre em Engenharia Química.

Dissertation presented to the School of Chemical Engineering as part of the requirements for the degree of Master in Chemical Engineering.

ESTE EXEMPLAR CORRESPONDE À VERSÃO FINAL DA DISSERTAÇÃO DEFENDIDA PELO ALUNO VICTOR DE BACKER MOURA E ORIENTADA PELO PROF. DR. MARCO AURÉLIO CREMASCO

_____

Prof. Dr. Marco Aurélio Cremasco

CAMPINAS

2018

Agência(s) de fomento e nº(s) de processo(s): CAPES, 33003017034P-8

Ficha catalográfica
Universidade Estadual de Campinas
Biblioteca da Área de Engenharia e Arquitetura
Luciana Pietrosanto Milla - CRB 8/8129

M865s

Moura, Victor de Backer, 1992-
Study of fluidization regimes by Shannon entropy / Victor de Backer Moura. – Campinas, SP : [s.n.], 2018.

Orientador: Marco Aurélio Cremasco.
Dissertação (mestrado) – Universidade Estadual de Campinas, Faculdade de Engenharia Química.

1. Fluidização. 2. Entropia. 3. Caracterização. 4. Processamento de sinais. I. Cremasco, Marco Aurélio, 1962-. II. Universidade Estadual de Campinas. Faculdade de Engenharia Química. III. Título.

Informações para Biblioteca Digital

Título em outro idioma: Estudo de regimes de fluidização pela entropia de Shannon
Palavras-chave em inglês:
Fluidization
Entropy
Characterization
Signal processing
Área de concentração: Engenharia Química
Titulação: Mestre em Engenharia Química
Banca examinadora:
Marco Aurélio Cremasco [Orientador]
Flávio Vasconcelos da Silva
Carlos Alexandre Moreira da Silva
Data de defesa: 05-02-2018
Programa de Pós-Graduação: Engenharia Química

Dissertação de Mestrado defendida por Victor de backer Moura e aprovada em 5 de fevereiro de 2018 pela banca examinadora constituída pelos doutores:

_____

Prof. Dr. Marco Aurélio Cremasco – Orientador

_____

Prof. Dr. Flávio Vasconcelos da Silva

_____

Prof. Dr. Carlos Alexandre Moreira da Silva

A Ata da defesa com as respectivas assinaturas dos membros encontra-se no processo de vida acadêmica do aluno

À minha mãe, Maria Angélica de Backer Lustosa, minha maior referência, e à Paola Visnardi Fassina, meu amor.

AGRADECIMENTOS

Agradeço à minha família pelo amor e apoio incondicional, em especial, à minha mãe, Maria Angélica de Backer Lustosa, que nunca deixou o meu lado, sempre acreditando em mim e abrindo os meus olhos para o melhor caminho.

À Paola Visnardi Fassina, que tanto amo, por me motivar e pelo carinho em todos os momentos.

Ao meu orientador, Prof. Dr. Marco Aurélio Cremasco, pela oportunidade, dedicação, apoio, confiança e paciência, tanto na execução desta dissertação quanto na supervisão do meu estágio docente. Seus ensinamentos com certeza não se restringem somente ao conteúdo deste trabalho.

Aos amigos Ivander Salvador Ruiz, Lucas Vilas Boas e Rafael Scatena pelo companheirismo, pela amizade e por deixar esta jornada muito mais agradável.

Aos amigos Carlos Eduardo Lima de Oliveira, Wesley Heleno Prieto e Wilson Murilo Correa da Silva Ferrari pela valiosa ajuda e prazerosa convivência.

Aos meus professores de graduação na UERJ e na University of Ottawa e da pós-graduação na Unicamp pela minha formação profissional e por me inspirarem a seguir na carreira acadêmica.

A Cachoeiro de Itapemirim, e a todos que lá estão, que, mesmo fisicamente distante, sempre permanceram em meus pensamentos.

À agência de fomento CAPES pelo apoio financeiro.

Enfim, a todos os que contribuíram direta ou indiretamente com este trabalho, o meu muito obrigado!

“The desire for knowledge shapes a man”.

Patrick Rothfuss

RESUMO

Leitos fluidizados têm sido amplamente utilizados em inúmeros processos industriais desde o seu uso no craqueamento catalítico do petróleo, em 1942. Devido ao alto grau de contato entre as fases, suas aplicações incluem recobrimento de partículas, combustão, secagem e síntese catalítica. No entanto, leitos fluidizados exibem dinâmica complexa e a caracterização de regimes de fluidização tem sido o foco de diversos estudos ao longo dos anos. Usualmente, monitora-se a pressão neste tipo de sistema, pois os instrumentos são robustos, relativamente baratos, não intrusivos e suportam condições operacionais severas. O presente trabalho avalia a entropia de Shannon para a análise de séries temporais de queda de pressão em um leito fluidizado gás-partícula. Esse parâmetro advém da teoria da informação, sendo uma medida da incerteza média de uma variável, e pode ser usado como uma ferramenta na caracterização de diferentes regimes de fluidização. Os dados experimentais usados nesta dissertação foram obtidos por Prieto (2014), sendo os experimentos realizados no Laboratório de Processos em Meios Porosos, na Unicamp. A fase fluida foi o ar atmosférico, a 25 ºC e a fase particulada consistia de microesferas de vidro pertencentes aos grupos A, B e D da classificação de Geldart. O carregamento de partículas no leito foram 400 e 800 g. O sistema de aquisição de pressão possui uma frequência de 1.000 Hz. A coluna foi construída em acrílico e possui um diâmetro interno e altura iguais a 10 e 100 cm, respectivamente. Dos resultados, percebeu-se que a entropia de Shannon é capaz de caracterizar a dinâmica dos regimes de fluidização embora haja uma dificuldade na identificação dos pontos de transição. No geral, existe um valor máximo na região próxima do ponto de mínima fluidização e, então, uma tendência decrescente é observada, a medida que o comportamento do leito se torna mais periódico no regime pistonado. Para que se possa calcular a entropia de Shannon, é necessário transformar a série temporal em uma distribuição de frequência. Devido ao fato de que este parâmetro é monotonicamente crescente com o número de classes de um histograma, cada série temporal teve o seu número de classes determinado individualmente. Os resultados estão de acordo com aqueles obtidos por Prieto (2014), que utilizou a análise no espaço de fase na caracterização da dinâmica do leito.

Palavras-chaves: *fluidização, entropia de Shannon, sinais de pressão, caracterização.*

ABSTRACT

Fluidized beds have been extensively used for numerous industrial processes since the catalytic cracking of petroleum in 1942. Due to the high level of contact between the phases, its applications include solid coating, combustion, drying and catalytic synthesis. However, fluidized beds exhibits complex dynamics and the characterization of fluidization regimes has been the subject of several studies along the years. Usually, pressure is the variable monitored in these systems, because the measurement instruments are robust, relatively cheap, virtually non-intrusive and can withstand harsh operational conditions. The present work evaluates the Shannon entropy for the analysis of pressure drop time series from a gas-particle fluidized bed. This parameter comes from the information theory, being a measure of average uncertainty of a random variable, and can be used as a tool for the characterization of different fluidization regimes. The experimental data used in this Dissertation were obtained by Prieto (2014). The experiments were performed at the Laboratory of Processes in Porous Media, at University of Campinas. The fluid phase was atmospheric air, at 25 ^{o}C and the particulate phase consisted of glass beads belonging to the A, B and D group of the Geldart classification. The total particle loads in the bed were 400 and 800 g. The column is made of acrylic with an inside diameter and height of 10 and 100 cm, respectively. The pressure acquisition system has a frequency of 1,000 Hz. As for the results, the Shannon entropy is capable of characterizing the dynamics of the fluidization regimes even if there is a certain difficulty in identifying the transition points. Generally, there is a maximum value around the region of the minimum fluidization and, then, a decreasing tendency of is observed as the behavior of the bed becomes more periodic in the slug flow regime. In order to calculate the Shannon entropy, it is necessary to transform the time series into a frequency distribution. Due the fact that this parameter is monotonically increasing with the number of classes of a histogram, each time series was analysed individually for the determination of their respective number of bins. The results are in accordance to those obtained by Prieto (2014), who used state space analysis to characterize the dynamics of the gas-particle fluidized bed.

Keywords: *fluidization, Shannon entropy, pressure signals, characterization.*

LIST OF FIGURES

LIST OF TABLES

NOMENCLATURE

Abreviation

PDF	Probability density function

Greek letters

α	Location parameter	[Pa]
β	Scale parameter	[Pa]
γ	Coefficient of skewness	[-]
γ_E	Euler-Mascheroni constant	[-]
Δ	Bin width	[Pa]
ΔP	Average differential pressure drop across the bed	[Pa]
$\Gamma(x)$	Gamma function of x	[-]
θ	Scale parameter	[Pa]
κ	Coefficient of kurtosis	[-]
λ	Scale parameter	[Pa]
μ	Mean	[Pa]
ρ	Density	[kg/m^3]
σ	Standard deviation	[Pa]
ψ	Digamma function of x	[-]

Capital letters

CV	Coefficient of variation	[-]
D	Supremum of the Kolmogorov-Smirnov test	[Pa]
D_c	Critical value of the supremum of the Kolmogorov-Smirnov test	[Pa]
$F(x)$	Cumulative distribution of a probability density function	[Pa]
H	Shannon entropy	[bits]
K	Conversion factor	[-]
N	Total number of points	[-]
$S(x)$	Experimental cumulative distribution	[Pa]
U	Superficial gas velocity	[m/s]
U_{mf}	Minimum fluidization velocity	[m/s]
X	Fourier transform of x	[Hz]

Minuscule letters

a	Scale parameter	[Pa]
b	Logarithm base	[-]
f	Frequency	[Hz]
$f(x)$	Probability density function of x	[-]
h	Differential entropy	[bits]
k	Shape parameter	[-]
m_r	Central moment of order r	[-]
n	Number of classes	[-]
$p(x)$	Probability of x	[-]
r	Order	[-]
s	Scale parameter	[Pa]
t	Time	[s]
x	Element of a pressure drop time series	[Pa]
$\overline{x^r}$	Moment of order r	[-]

CONTENTS

1. INTRODUCTION

Gas-particle contacting is a form of mixing that is done for a variety of reasons, including to effect mass and heat transfer, chemical reactions and drying applications (Cheremisinoff, 2000). Since fluidization hit the industrial scene in 1942 with catalytic cracking, it has moved into many other areas, because of its high level of contact between the phases (Kunii and Levenspiel, 1991). The complex dynamics of this unit operation stimulated numerous studies on the subject, in order to develop techniques capable of understand the phenomenon occurring inside the bed (Green and Perry, 2008). Therefore, the necessity of monitoring the operational conditions of a fluidized bed, in the interest of maintaining a specific fluidization regime and, by extension, the heat and mass transfer at a desired rate.

Several methods have been proposed for the characterization of fluidization regimes: visual observations, study of time averaged entities, such as the axial solids concentration profile and interpretation of fluctuating signals from in-bed measurements. For a qualitative classification of regimes, visual observation is important, but also subjective in nature. For instance, what is regarded to be a turbulent regime by some observers may be described as bubbling by others. Methods based on the study of time averaged values of solids concentration do not directly quantify the flow dynamics and may lead to pitfalls. On the other hand, a quantitative description of flow regimes can be obtained from time series analysis of fluctuating signals of in-bed measurements of pressure or of other signals, such as local solids concentration, from optical and capacitance probes. It is important to mention that an appropriate measurement method as well as appropriate methods of time series analysis are the key for such quantification. Pressure is commonly used to characterize fluid dynamics of gas-particle fluidized beds mainly because it is a robust, cheap and easily measured parameter. Nonetheless, the interpretation of pressure signals is not straightforward and, therefore, there are many different ways to analyse them, which can basically be grouped into three main categories – the time domain methods, frequency domain methods and state space methods (Johnsson et al., 2000).

Among the methods mentioned previously, time and frequency domain techniques, such as the standard deviation and the Fourier transform, respectively, have been traditionally used to study pressure signals (van Ommen et al., 2011). Space state methods, also known as the chaotic approach, applied to the study of fluidization only begun in the 90's, with a group at the Delft University of Technology, in Netherlands. The results rapidly showed that chaotic

invariants could be an interesting alternative to the conventional analysis in order to characterize fluidization regimes and they have been extensively used ever since. For instance, the complex and nonlinear gas-particle interaction of a fluidized bed exhibits a continuous power spectrum, when the Fourier transform is applied to a pressure drop time series. Since the spectral analysis intends to identify a dominant frequency, correspondent to the phenomenon, a continuous spectrum emerges as a difficulty for that. As for the state space method, there is no need for a clean power spectrum, in fact, Ferrara and Prado (1994) claims that because of the aperiodic behavior of chaotic time series, the continuous power spectrum serves as proof of chaotic dynamics.

This Dissertation follows the previous studies of fluidized bed time series in the Laboratory of Processes in Porous Media, at the University of Campinas. Castilho (2007) studied the volumetric concentration of solids using the standard deviation of the electrical signals from an optical fiber probe. In 2011, the same author presented a thesis applying the chaos theory in a circulating fluidized bed by measuring electrical signals. Prieto (2014), also used the state space methodology, but on pressure drop time series from a fluidized bed. This work will focus on complementing those analysis by applying a different method. It has a statistical approach to pressure drop time series from a fluidized bed. In order to do so, the Shannon entropy was evaluated as a parameter for the characterization of fluidized bed dynamics.

Shannon entropy is a measure of average uncertainty of a random variable. It comes from the information theory and it is calculated from a frequency distribution (Baltzer et al., 2015). This parameter, thus, measures the complexity of a system from its amount of information and uncertainty, which could bring useful results in the attempt to characterize the elusive nature of fluidized beds (Wang et al., 2017). The moments of a time series or a frequency distribution describe the shape of its set of points. The first moment is the arithmetic mean, and the second central moment is the variance, which describes how the data points are dispersed around the first one (Correa, 2003; Spiegel and Stephens, 2008). Different time series have different frequency curves, and by that, necessarily different moments, which leads to the premise that their fluidization regimes can be distinct by these quantities and the Shannon entropy. Nonetheless, in order to transform a time series into a frequency distribution, to eventually evaluate the Shannon entropy, it is necessary to determine the number of bins that will group the data.

Therefore, the attention in this work has been directed to the development and testing of statistical analysis for fluidized beds by calculating the Shannon entropy. The final objective is to evaluate this method as an alternative for fluidization regime identification.

1.1 General objective

The main objective of this Dissertation is to identify fluidization regimes in a fluidized bed through the analysis of the experimental pressure drop time series, obtained by Prieto (2014), via a statistical approach, using the Shannon entropy.

1.2 Specific objectives

This work has the following specific objectives:

- Analysis of the original experimental time series in order to construct the fluidization curve for each particulate phase;
- determine the number of bins which each time series are going to be divided into by evaluating the coefficient of variation;
- transform each time series into frequency distributions with their respective optimal number of bins;
- calculate the Shannon entropy from the frequency distributions;
- fit the experimental frequency distribution in different families of continuous probability distributions, evaluating them with the Kolmogorov-Smirnov test and the sum of the squared errors;
- characterize the fluidization regimes by the Shannon entropy;

2. LITERATURE REVIEW AND THEORETICAL FOUNDATION

2.1 Literature review

2.1.1 Gas-particle fluidization

Fluidized beds basically consist of a suspension of particles submitted to an ascending flow of the fluid phase in a vertical channel (Cremasco, 2014). Although the particles remain in contact with each other through collisions, the interparticle friction is small and the particulate phase is transformed into a fluid like state (Kunii and Levenspiel, 1991; Vander Stappen, 1996). This technique was first used industrially in the Winkler's process for the gasification of coal, in the early 1930's. However, it was only around the beginning of the Second World War that it developed and spread, primarily because of its application in the catalytic cracking of petroleum (Yates, 1983). Currently, due to their high level of contact between gases and solids, which promotes high rates of heat and mass transfer, fluidized beds are employed in numerous industrial processes, such as solid coating, combustion, drying and catalytic synthesis (Green and Perry, 2008; Cremasco, 2014).

The behavior of fluidized bed systems can be described from the properties of the fluidized particles and the flow regimes. Measurements of the pressure drop across the bed can be used to identify the minimum fluidization velocity, for instance. Figure 2.1 shows the classical relationship of pressure drop through the bed versus the superficial gas velocity. For low gas velocities, the fluid merely percolates through the voids between packed particles while they remain motionless, characterizing the packed bed regime. With increasing superficial gas velocity, the pressure drop through the bed also increases, reaching a peak. The frictional drag force causes the particles to rearrange, which can alter the bed voidage. The gas velocity at which the peak occurs is called the minimum fluidization velocity, and it equals the weight of the bed divided by the cross-sectional area of the column. Upon rearrangement, the pressure decreases until it drops to a constant. To explain this result, note that the gas-particle phase is well aerated and can deform easily without appreciable resistance, similar to the hydrodynamic behavior of a liquid. If a gas is introduced at the bottom of a tank containing a liquid of low viscosity, the pressure required for injection is roughly the static pressure of the liquid and is independent of the gas flow rate. Finally, as the velocity decreases, the pressure drop follows a different path without passing through the peak. This hysteresis effect is due to the expansion

of the bed, that is, the different voidage resultant from the rearrangement of the particles (Kunii and Levenspiel, 1991; Fan and Zhu, 1998).

Figure 2.1 – Pressure drop variation with the gas velocity (Fan and Zhu, 1998).

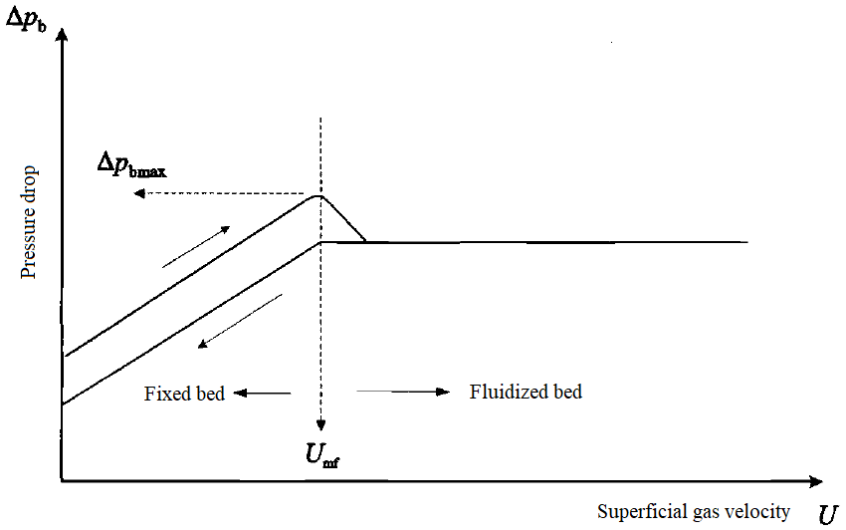

As it was discussed, the fluid dynamics behavior of the bed varies with the gas flow rate. Specifically, fluidization regimes go from the packed bed to the particulate, bubbling, slug flow, turbulent, fast fluidization and pneumatic conveying transport regime (Green and Perry, 2008), as illustrated in Figure 2.2.

Figure 2.2 – Gas-particle fluidization regimes (adapted from Grace, 1986).

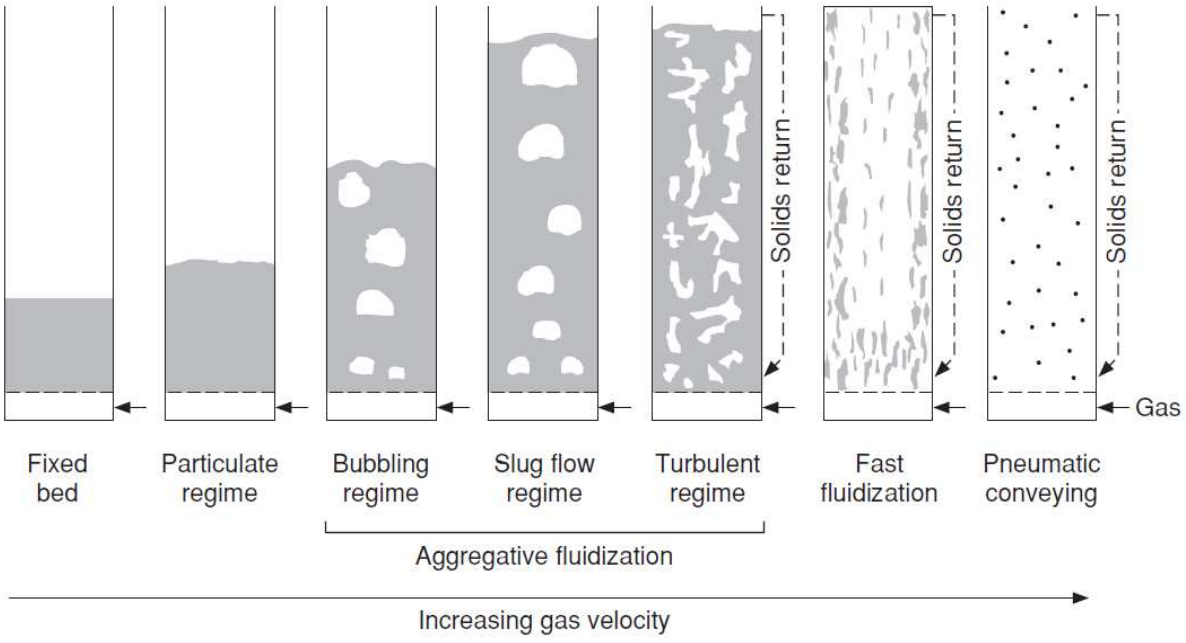

In the bubbling fluidization regime, bubble coalescence and breakup take place, inducing a vigorous motion of the particles. As the velocity increases, so does the tendency of bubble coalescence (Fan and Zhu, 1998). Once their size becomes large enough, the bed will slug. The slugging fluidized bed is characterized by severe pressure fluctuation and limited solids mixing. The turbulent regime occurs when the gas velocity is higher than the terminal velocity of the particle, with stable bubbles breaking down into unstable voids that continuously disintegrate and reform. If the gas velocity is increased further, the bed transitions to the dilute-phase transport, which are the fast fluidization and pneumatic conveying regimes (Green and Perry, 2008).

It is worth to emphasize that some of these regimes in Figure 2.2 does not form, depending on the particle properties that is fluidizing. Therefore, Geldart (1973) proposed a classification for different particles, based on their fluidization behavior. Geldart's classification was obtained empirically and has been widely adopted in research and design of fluidized beds. Figure 2.3 presents this classification, where particles are classified in terms of the density difference between the phases and the particle diameter.

Figure 2.3 – Geldart's classification (Geldart, 1973).

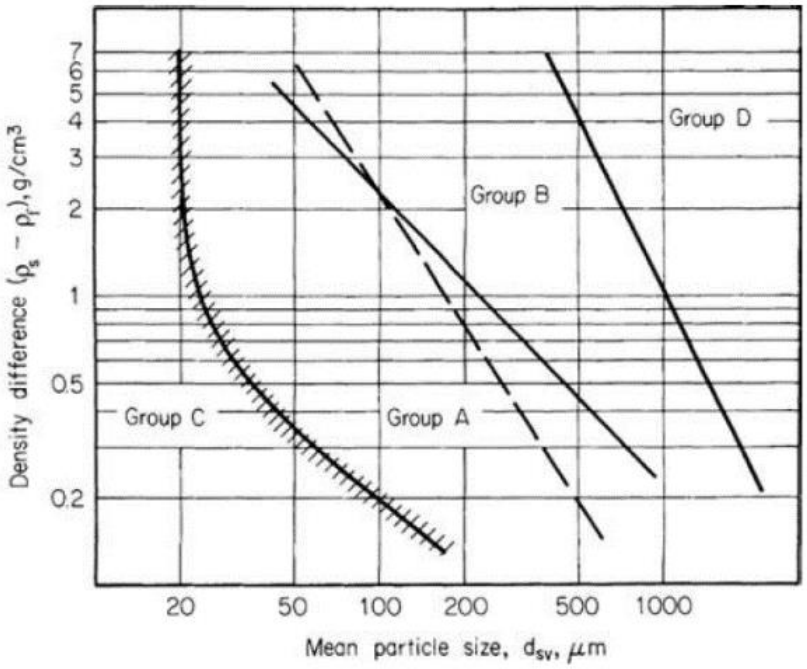

Group A particles expand considerably after the minimum fluidization and prior to the commencement of bubbling regime. One example is cracking catalyst. Those in group B bubble at the minimum fluidization velocity. The bubble size increases with the bed height and

bed expansion is moderate. Sand is the most typical powder. Category C comprises small particles which are cohesive, such as flour and starch. They are difficult to fluidize and gas channeling is the most common characteristic when fluidizing these particles. Finally, the ones in group D are of large size or density, or both, and spout readily. Also, the bed expansion is low and the particle mixing is not as good as that for group A and B particles. Drying grains and peas, roasting coffee beans and some roasting metal ores fall into this category (Geldart, 1973; Kunii and Levenspiel, 1991; Fan and Zhu, 1998; Cremasco, 2014).

Furthermore, Grace (1986) has correlated various types of gas-particle systems, in which the gas is flowing vertically upward in a status graph using the Archimedes number for the particle size and a nondimensional velocity for the gas effects, as shown in Figure 2.4. This diagram can be used as a guide to estimate the fluidization regime for various particle sizes and operating conditions. Nonetheless, it should not be substituted for more exact methods of determining the actual fluidization regime (Green and Perry, 2008).

Figure 2.4 – Simplified fluidization status graph (adapted from Grace, 1986).

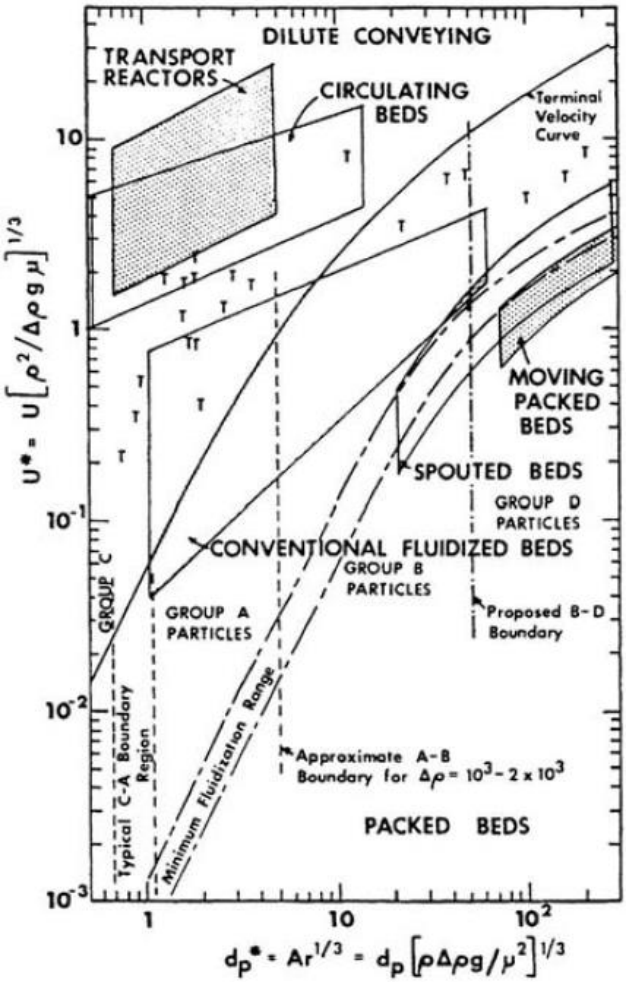

2.1.2 Pressure drop time series analysis

Pressure is often chosen to characterize fluid dynamics of gas-particle fluidized beds due to its advantage of being easily measured, even when the operational conditions are harsh, such as in industry. Additionally, the pressure measurement system is robust, relatively cheap and virtually non-intrusive (van Ommen et al., 2011). De Martín et al. (2010) also reasons that pressure is mostly used because of the quality and quantity of information in low frequency signals.

In the study of fluidized beds, it is common to plot the fluidization curve of the system, that is, the pressure drop versus the gas velocity, such as that one presented in Figure 2.1. However, for a fixed velocity, the data obtained exhibits temporal variation around a mean value (Prieto, 2014). Hence, the data set collected can be classified as a pressure drop time series, as it is a series of data points ordered in time (Morettin and Toloi, 2006). Figure 2.5 shows an example of fluidization time series.

Figure 2.5 – 40,000 points time series for the minimum fluidization of group B glass beads with 0.8 kg particle load (Prieto, 2014).

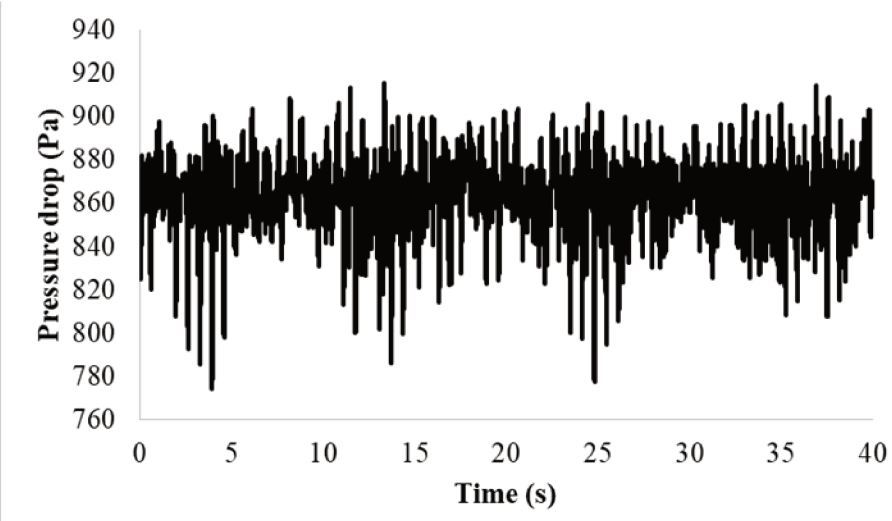

Then, if *x(N)* is a time series with *N* equidistant points in time, the average is given by Equation 2.1 (Spiegel and Stephens, 2008).

$$\bar{x} = \frac{\sum x}{N} \tag{2.1}$$

An example of an experimental fluidization curve is displayed in Figure 2.6. It was obtained by Prieto (2014) and it depicts the pressure drop versus the normalized gas velocity for the fluidization of glass beads belonging to the B group of the Geldart classification with a total particle load in the bed of 0.8 kg. Each point in the plot of Figure 2.6 corresponds to the average value of a pressure drop time series.

Figure 2.6 – Fluidization curve of group B glass beads with 0.8 kg particle load (Prieto, 2014).

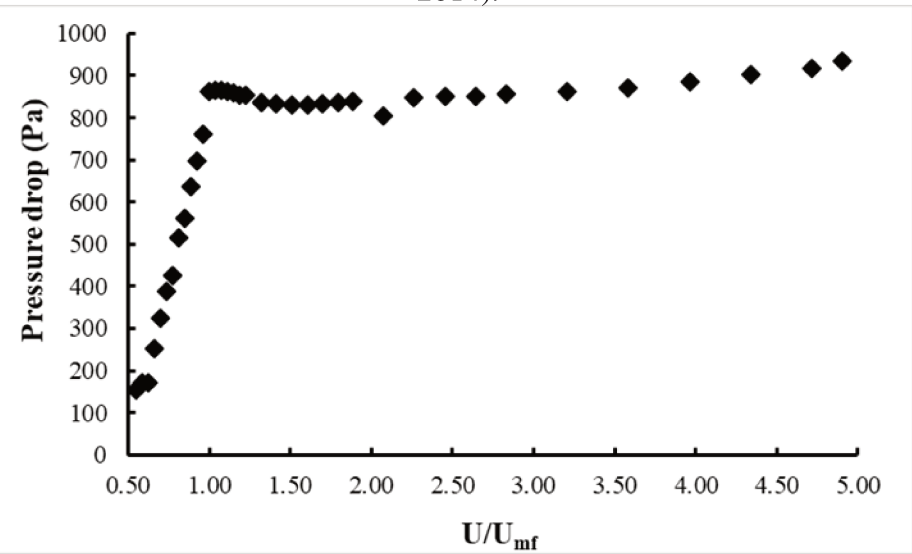

A widely applied method (see Table 2.1) is to determine the amplitude of the pressure signals, expressed in the form of standard deviation, as defined in Equation 2.2.

$$\sigma = \sqrt{\frac{\sum(x - \bar{x})^2}{N}} \tag{2.2}$$

Time series can be classified as stochastic, deterministic or chaotic. A stochastic time series is unpredictable in a given time interval, showing randomness in its temporal evolution. Therefore, they are considered to be nonlinear. On the other hand, deterministic time series have a linear temporal evolution and their trajectory can be predicted in the short and long term. In multiphase systems, like gas-particle fluidized beds, the pressure drop evolution with increments of gas velocity is predictable, when assessed with averaged terms. However, evaluating the fluidization regimes separately, the time series displays chaotic behavior, which is a combination of stochastic and deterministic systems. The main properties of a chaotic time

series are nonlinearity, aperiodicity and high sensitivity to initial conditions (Ferrara and Prado, 1994; Monteiro, 2011).

Thus, depending on the final objective of the analysis, the average value of the time series can be enough, which is the case when constructing the fluidization curve. Conversely, for a deeper understanding of the phenomenon, the whole time series and how the points are ordered in time are crucial, for these purposes, it can be used the analysis using the Fourier transform or a chaotic approach. Consequently, Literature presents a large number of methods for the analysis of pressure drop time series, which can be grouped into three categories: time domain, frequency domain, and state space (Vander Stappen, 1996; Johnsson et al., 2000; van Ommen et al., 2011).

The ensuing topics will briefly discuss studies of fluidized beds in these three categories.

2.1.2.1 Time domain analysis

There are several studies of fluidized beds using time domain analysis of signals Table 2.1 presents some examples related to process engineering.

Table 2.1 – Time domain analysis of fluidized beds time series.

Authors	Equipment	Objectives
Chong et al. (1987)	Fluidized bed	Control the quality of fluidization using the variance of pressure drop time series.
Kai and Furusaki (1987)	Fluidized bed reactor	Evaluate and improve the quality of fluidization in the methanation of carbon dioxide by studying the standard deviation in pressure signals.
Saxena et al. (1993)	Fluidized bed	Calculate the coefficients of skewness and kurtosis of pressure signals in order to establish diagnostic procedures for the quality of fluidization in gas-particle systems.
Wilkinson (1995)	Fluidized bed	Determination of the minimum fluidization velocity using the standard deviation of pressure fluctuations.
Bi et al. (2000)	Fluidized bed	Identify the transition velocity from the bubbling to turbulent regime. The authors concluded that a maximum in the standard deviation as a function of the superficial gas velocity indicated this turning point.

Table continued

Authors	Equipment	Objectives
van Ommen et al. (2004)	Fluidized bed	Detect defluidization in gas-particle fluidized bed by monitoring the standard deviation of pressure fluctuations with decreasing gas velocity.
Puncochar and Drahos (2005)	Fluidized bed	Determine the minimum fluidization velocity using the standard deviation of pressure fluctuations and spectral analysis.
Castilho (2007)	Circulating fluidized bed – riser	Study the volumetric concentration of solids using the standard deviation of signals from an optical fiber probe.
Felipe and Rocha (2007)	Fluidized bed	Predict the minimum fluidization velocity using the standard deviation of pressure signals.
Davies et al. (2008)	Fluidized bed	Estimate the particle size in a fluidized bed using the standard deviation of pressure drop time series.

The standard deviation is the square root of the variance. The analysis of this parameter has the advantage of its fast calculation (Johnsson et al., 2000; van Ommen et al., 2011). Notice how the majority of these references work with the standard deviation as opposed to higher-order moments, that is, the coefficients of skewness and kurtosis.

Another typical time domain analysis is to transform a time series into a frequency distribution. This curve contains the frequency or the count of occurrences of values in a particular interval. It is a form of evaluating how the signals are distributed around the mean, which can qualitatively indicate the flow uniformity, for instance (Castilho, 2011).

The method of moments, which includes parameters such as the standard deviation, coefficient of skewness and coefficient of kurtosis, is the main type of analysis in time domain. Moreover, only when transforming a time series into a frequency distribution that is possible to evaluate the Shannon entropy.

2.1.2.2 Frequency domain analysis

Any temporal evolution of a dynamic system can be expressed as a sum of many individual frequency components. Eventually, the number of components can be infinite. The determination of the weight that each of these components have in the original function is called spectral analysis (Ferrara and Prado, 1994). One of the most applied methods to pressure signals

in the frequency domain is the power spectrum. It uses the Fourier transform to obtain the dominant frequency, which can provide identification and monitoring of the various fluidization regimes (Johnsson et al., 2000; van Ommen et al., 2011). The Fourier transform of a function *x(t)* is defined as (Ferrara and Prado, 1994)

$$X(f) = \int_{-\infty}^{\infty} x(t) e^{-i2\pi f t} dt \tag{2.3}$$

Through Equation 2.3, the data collected goes from the time domain to the frequency domain. Table 2.2 exhibits some works that have used the frequency domain analysis in the study of fluidization.

Table 2.2 – Frequency domain analysis of fluidized beds time series.

Authors	Equipment	Objectives
Kage et al. (2000)	Fluidized bed	Detection of fluidization states by analysing pressure fluctuations measured at the plenum chamber using the Fourier transform to obtain the power spectrum.
Trnka et al. (2000)	Fluidized bed	Online characterization of the state of a fluidized bed using the Fourier transform on pressure signals.
Brown and Brue (2001)	Fluidized bed	Determination of the power spectrum of pressure drop time series in order to understand the dynamical behavior of fluidized beds.
Felipe (2004)	Fluidized bed	Monitoring typical fluidization regimes of gas-particle bubbling columns by the power spectra obtained via the Fourier transform from pressure drop time series.
Butzge (2012)	Spouted bed	Use the dominant frequency to monitor and control the fluid dynamics regime in a spouted bed wetting process.
Jaiboon et al. (2013)	Circulating fluidized bed	Study the effect of superficial gas velocity on the average frequency and average intensity of the power spectrum in a gas-particle fluidization system.
Gyan (2015)	Fluidized bed	Analysis of pressure fluctuations by the power spectra of fluidized bed columns having different internal diameters.
Bae et al., (2017)	Fluidized bed	Investigate bubble flow characteristics in a gas-particle fluidized bed by power spectrum analysis of absolute pressure fluctuations.

Analysis in the frequency domain is a common tool for investigating pressure signals recorded in fluidized beds. This type of analysis is typically carried out using the Fourier transform. However, a recently introduced method into the analysis of fluidized beds dynamics is the wavelet analysis. Wavelets provide an approach to signal processing which allows for the representation of a signal simultaneously in time and in frequency (van Ommen et al., 2011). Likewise the Fourier transform, which decomposes the signal into a family of complex sinusoids, the wavelet transform decomposes the signal into a family of wavelets. In order to define what a wavelet is, Burrus et al. (1998) define a wave as an oscillating function of time and space, thus, a wavelet is a "small wave", which has its energy concentrated in time. Table 2.3 displays studies using the wavelet analysis in fluidization systems.

Table 2.3 – Wavelet analysis of fluidized beds time series.

Authors	Equipment	Objectives
Briens et al. (2003)	Fluidized bed reactor	Online detection of the bed fluidity through the ratio between small and large pressure fluctuations, via the wavelet analysis.
Sasic et al. (2006)	Fluidized bed	Analysis of pressure fluctuations in a gas-particle system using the wavelet analysis in order to acquire information about bubbles in different scales of the wavelet transform.
Wu et al. (2007)	Fluidized bed	Use the wavelet transform to compute the average cycle time in order to differentiate fluidization behavior between different particle systems.
Chen and Chen (2008)	Fluidized bed reactor	Determination of the average particle size in a fluidized bed reactor by using a wavelet based neural network in acoustic emission signals.
Yang and Leu (2008)	Circulating fluidized bed	The wavelet analysis helped mark the transition velocity to the slug flow regime and discriminate the bubble growth dynamics of different kinds of particles in different flow regimes.
Silva (2015)	Fluidized bed	Showed that the wavelet transform presents a vast application in processes that occur regime changes due to influence of humidity and the different scale phenomena that happen during regime transitions in solid coating could be better discretized.

In fluidized beds, the major frequency content of pressure fluctuations is normally below 10 Hz. Most works, dealing with frequency domain analysis, aims to identify dominant frequencies (Johnsson et al., 2000). However, according to Ferrara and Prado (1994), the aperiodic behavior of a chaotic time series results in a continuous power spectrum. Stringer (1989) was the first to claim that a gas-particle fluidized bed is a chaotic system. Hence, it is in this scenario that chaos theory is inserted in the analysis of pressure drop time series from a fluidized bed, because it dismisses the requirement of a clean power spectrum (Prieto, 2014).

2.1.2.3State space analysis

Complementing analysis in the time and frequency domain, the fluidized bed pressure signal can be studied in the state phase (Johnsson et al., 2000; van Ommen et al., 2011). This approach is common for nonlinear analysis and became popular after the pioneering work by Stringer (1989). Since then, chaos analysis has been extensively applied in pressure drop time series. Table 2.4 presents some examples that have used the state space method in the study of fluidized beds.

Table 2.4 – State space analysis of fluidized beds time series (adapted from Castilho, 2011).

Authors	Equipment	Objectives
Daw et al. (1990)	Fluidized bed	Evaluate the dynamics of a gas-particle fluidized bed by reconstructing the attractor and calculating its dimensions.
van den Bleek and Schouten (1993)	Fluidized bed	Use the chaotic approach to assess time series obtained from a theoretical model of a fluidized bed. The results were compared with experimental data.
Vander Stappen (1996)	Fluidized bed	Characterize the dynamics in a fluidized bed system using the Kolmogorov entropy and correlation dimension as a function of the operational conditions.
Ji et al. (2000)	Circulating fluidized bed	Study the dynamic behavior of the particle-fluid flow in a circulating fluidized bed by chaotic analysis of pressure, local heat transfer and voidage fluctuations.
Chaplin et al. (2004)	Fluidized bed dryer	Track the moisture content within the bed using a statistical test, *S*-statistics, between chaotic attractors for fluidized systems.

Table continued

Authors	Equipment	Objectives
Briongos et al. (2006)	Fluidized bed	Demonstrate that measurements of low frequency out-bed passive acoustic emissions are useful for monitoring gas-particle fluidized bed dynamics. Neither time nor frequency domain analysis seemed able to fully characterize the bed dynamics, only the chaotic approach.
Zarghami et al. (2008)	Fluidized bed	Prediction of pressure fluctuations is fluidized beds in two different hydrodynamic states using nonlinear techniques.
Breault et al. (2012)	Circulating fluidized bed - riser	Characterize flow conditions and characteristic scales in a circulating fluidized bed by analyzing the raw voltage signal from a fiber optic probe.
Prieto (2014)	Fluidized bed	Application of state space analysis in a fluidized bed with particles A, B and D of the Geldart classification.
Ziaei-Halimejani et al. (2017)	Fluidized bed	Analyze the hydrodynamics of a gas-particle fluidized bed from its pressure fluctuation using cross recurrence quantification analysis.

The next topic is about the Shannon entropy. This parameter can be associated with the complexity of a particulate system but it is still not much employed in fluidization studies, ergo, the proposal of this Dissertation to evaluate it for the characterization of fluidized bed regimes.

2.2 Theoretical foundation

2.2.1 Shannon entropy

Shannon (1948) proposed an expression for a quantity, H, in order to measure how much "choice" is involved in the selection of an event or of how uncertain of the outcome one can be, given the set of possible events and their probabilities of occurrence. Let $p(x)_i$ be the probability of x_i occurring. Thus, it is reasonable to require of H the following properties (Shannon, 1948):

- H should be continuous in the $p(x)_i$.

- If all probabilities are equal, that is, $p(x)_i = 1/n$, with n being the number of possible events, then H should be a monotonic increasing function of n. With equally likely events there is more choice, or uncertainty, when there are more possible events.

The Shannon entropy is then defined in the form of Equation 2.4.

$$H = -K\sum_{i=1}^{n} p(x_i) log_b p(x_i) \tag{2.4}$$

where K is a positive constant that amounts to a choice of a unit of measure.

The parameter H play a central role in information theory as measures of information, choice and uncertainty (Shannon, 1948). When b is equal to 2, the units of entropy are bits (Guo et al., 2002). Also, since $p(x)$ is a probability distribution function, the probability that at least one of the elementary events in the entire sample space will occur is certain. Therefore, Equation 2.5, which is a probability axiom, must be satisfied (Bulusu and Plesniak, 2015).

$$\sum_{i=1}^{n} p(x_i) = 1 \tag{2.5}$$

Thus, for K equal to one and the entropy with the units of bits, Equation 2.4 is rewritten as

$$H = -\sum_{i=1}^{n} p(x_i) log_2 p(x_i) \tag{2.6}$$

Shannon entropy quantifies the average unpredictability in a random variable. Hence, the higher the entropy, the lower the information content of the time series (Baltzer et al., 2015). If one predicts the outcome exactly before it happens, the probability will be a maximum value and, as a result, the Shannon entropy will be a minimum value. If one is absolutely able to predict the outcomes of an event, then, Shannon entropy will be zero (Cai et al., 2013).

Although Shannon proposed this quantity over sixty years ago, only recently, studies of this parameter have been used to characterize fluidization regimes (Zhong and Zhang,

2005; Zhong et al., 2009; Duan and Cong, 2013; Cremasco et al., 2017; Wang et al., 2017). The main objective of this Dissertation is to evaluate the Shannon entropy in the fluidization of particles A, B and D of the Geldart classification. For that, it is necessary to simply apply Equation 2.6 to the grouped data, as the relative frequency of a class can be interpreted as the probability of any element from that class occurring.

It is important to mention that Shannon defined Equation 2.4 for the case of a discrete variable. However, the concept of entropy for continuous distributions was also presented in Shannon's original paper (Shannon, 1948) and is referred to as the differential entropy or Shannon's differential entropy. Therefore, for a continuous random variable *X* with a probability density function (PDF) *f(x)*, the differential entropy is given by Equation 2.7 (Michalowicz et al., 2013).

$$h = -\int_{-\infty}^{\infty} f(x) \log_2 f(x)\, dx \tag{2.7}$$

The natural approach to deriving continuous entropy would be to take discrete entropy in the limit of *n*, the number of bins in a frequency distribution, that is, extending the discrete case towards infinity. This is equivalent to defining integrals in calculus using a Riemannian approach. Yet, the notion of "average uncertainty" carried by Equation 2.4 cannot be extended to its differential correspondent. Instead, differential entropy is rather a function of the parameters of a distribution that describes how uncertainty changes as the parameters are modified (Santamaría-Bonfil et al., 2016).

Thus, alternatively to calculating the Shannon entropy directly from the frequency distribution, it is possible to use theoretical probability density functions and fit the experimental frequency distribution into these models. The best fit will be the one with the smallest difference between the experimental and theoretical distribution. Once the model is selected, its differential entropy can be readily calculated using a formula displayed in Table 2.6.

Table 2.5 presents the theoretical probability density functions that was used in this Dissertation. These expressions were all retrieved from Lazo and Rathie (1978) and Crooks (2017). According to Mun (2008), the process of selecting the correct probability distribution starts with plotting the data, in order to observe characteristics such as the presence or absence of symmetry, and basically select a distribution whose characteristics match those of the variable in question. Since this fitting process is basically empirical, the theoretical probability

functions presented in Table 2.5 were chosen due to their diversity. For instance, the Normal and the Cauchy distribution are symmetric while the log-Normal skews to the right and the Weibull, to the left. Moreover, distributions such as the Gamma, Beta and Pearson are flexible, depending on the combination of their parameters. Lastly, as mentioned previously, the distribution that exhibits the smallest error from the experimental data are elected as the best fit.

Table 2.5 – Theoretical probability density functions (Lazo and Rathie, 1978; Crooks, 2017).

Distribution	***f(x)***	**Parameters**
Normal	$\frac{1}{\sqrt{2\pi\sigma^2}} exp\left[-\frac{(x-\mu)^2}{2\sigma^2}\right]$ (2.8)	μ: mean σ^2: variance
log-Normal	$\frac{1}{\sqrt{2\pi x^2\sigma^2}} exp\left[-\frac{(ln(x)-\mu)^2}{2\sigma^2}\right]$ (2.9)	μ: mean σ^2: variance
Logistic	$\frac{exp\left(-\frac{x-\mu}{s}\right)}{s\left[1+exp\left(-\frac{x-\mu}{s}\right)\right]^2}$ (2.10)	μ: mean s: scale parameter
Gumbel	$\left(\frac{1}{\beta}\right) exp\left\{-\left(\frac{x-\alpha}{\beta}\right) - exp\left[-\left(\frac{x-\alpha}{\beta}\right)\right]\right\}$ (2.11)	α: location parameter β: scale parameter
Weibull	$\left(\frac{k}{\lambda^k}\right) x^{k-1} exp\left[-\left(\frac{x}{\lambda}\right)^k\right]$ (2.12)	λ: scale parameter k: shape parameter
Gamma	$\frac{x^{k-1}}{\theta^k \Gamma(k)} exp\left(-\frac{x}{\theta}\right)$ (2.13)	θ: scale parameter k: shape parameter $\Gamma(k)$: gamma function of k
Beta	$\frac{\Gamma(\alpha+\beta)}{\Gamma(\alpha)\Gamma(\beta)} x^{\alpha-1}(1-x)^{\beta-1}$ (2.14)	α: shape parameter β: shape parameter $0 \leq x \leq 1$
Pearson III	$\frac{1}{\theta\Gamma(k)}\left(\frac{x-\alpha}{\theta}\right)^{k-1} exp\left[-\frac{(x-\alpha)}{\theta}\right]$ (2.15)	α: location parameter θ: scale parameter k: shape parameter
Exponential	$\frac{exp\left(-\frac{x}{\lambda}\right)}{\lambda}$ (2.16)	λ: scale parameter

Table continued

Distribution	*f(x)*	Parameters
Maxwell	$\sqrt{\frac{2}{\pi}}\left(\frac{x^2}{a^3}\right)exp\left(-\frac{x^2}{2a^2}\right)$ (2.17)	a: scale parameter
Rayleigh	$\left(\frac{x}{a^2}\right)exp\left(-\frac{x^2}{2a^2}\right)$ (2.18)	a: scale parameter
Cauchy	$\left(\frac{\gamma}{\pi}\right)\frac{1}{\gamma^2+x^2}$ (2.19)	γ: scale parameter
Chi-square	$\frac{x^{n/2-1}}{2^{n/2}\Gamma(n/2)}exp\left(-\frac{x}{2}\right)$ (2.20)	n: positive integer

The gamma function $\Gamma(x)$, used in the Gamma, Beta and Pearson III distribution, is defined as

$$\Gamma(x) = \int_0^\infty t^{x-1}exp(-t)dt \tag{2.21}$$

Table 2.6 displays the differential entropy of the probability density functions in Table 2.5. Notice that most of the probability density functions have Euler's number in their formula. Therefore, for the sake of simplification, instead of using the base of logarithm b equals to 2 in Equation 2.7, which would result in an entropy with units of bits, the base selected is the Euler's number, resulting, consequently, in an entropy with units of nats. This mathematical artifice intends to exploit the property that the natural logarithm of Euler's number is equal to 1. It is worth mentioning that this change in base comes without prejudice to the final result. In order to convert the differential entropy with units of nats to bits, it is only necessary to multiply this former parameter by a conversion factor equals to ln(2). The relation between the differential entropy with units of nats and with units of bits is given by Equation 2.22

$$H[bits] = H[nats] \times \ln(2) \tag{2.22}$$

Additionally, Table 2.6 brings the Euler-Mascheroni constant (γ_E), which is equal to, approximately, 0.57721 (Lazo and Rathie, 1978) and the digamma function $\psi(x)$, expressed in Equation 2.23 (Crooks, 2017).

$$\psi(x) = \frac{\Gamma'(x)}{\Gamma(x)} \tag{2.23}$$

Abramowitz and Stegun (1972) presents an approximation for the digamma function, according to Equation 2.24.

$$\psi(x) = \ln(x) - \frac{1}{2x} - \frac{1}{12x^2} + \frac{1}{120x^4} - \frac{1}{252x^6} + \frac{1}{240x^8} - \frac{5}{660x^{10}} + \frac{691}{32760x^{12}} \tag{2.24}$$

The latter is the beginning of the asymptotical expansion of $\psi(x)$. Beal (2003) suggests using this expansion with terms above x^{12} cut off, which yields a precision of at least 12 digits, except near the zeroes. Moreover, for x smaller than 6, it is recommended to use a property of the digamma function, explicit in Equation 2.25, in order to shift x to a value greater than 6.

$$\psi(x+1) = \frac{1}{x} + \psi(x) \tag{2.25}$$

Table 2.6 – Differential entropy of theoretical probability density functions (Lazo and Rathie, 1978; Crooks, 2017).

Distribution	***h* [nats]**	**Parameters**
Normal	$\frac{1}{2}\ln(2\pi e\sigma^2)$ (2.26)	σ^2: variance
log-Normal	$\mu + \frac{1}{2}\ln(2\pi e\sigma^2)$ (2.27)	μ: mean σ^2: variance
Logistic	$\ln(s) + 2$ (2.28)	s: scale parameter
Gumbel	$\ln(\beta) + \gamma_E + 1$ (2.29)	β: scale parameter
Weibull	$\ln\left(\frac{\lambda}{k}\right) + \frac{(k-1)\gamma_E}{k} + 1$ (2.30)	λ: scale parameter k: shape parameter

Table continued

Distribution	***h* [nats]**	**Parameters**
Gamma	$\ln[\theta\Gamma(k)] + (1-k)\psi(k) + k$ (2.31)	θ: scale parameter k: shape parameter $\Gamma(k)$: gamma function of k $\psi(k)$: digamma function of k.
Beta	$\ln\left[\frac{\Gamma(\alpha)\Gamma(\beta)}{\Gamma(\alpha+\beta)}\right] - \psi(\alpha)(\alpha-1) - \psi(\beta)(\beta-1) + \psi(\alpha+\beta)(\alpha+\beta-2)$ (2.32)	α: shape parameter β: shape parameter $0 \leq x \leq 1$
Pearson III	$\ln\big(\theta\Gamma(k)\big) + (1-k)\psi(k) + k$ (2.33)	θ: scale parameter k: shape parameter
Exponential	$\ln(\lambda) + 1$ (2.34)	λ: scale parameter
Maxwell	$\ln\big(a\sqrt{2\pi}\big) + \gamma_E - \frac{1}{2}$ (2.35)	a: scale parameter
Rayleigh	$\ln\left(\frac{a}{\sqrt{2}}\right) + \frac{\gamma_E}{2} + 1$ (2.36)	a: scale parameter
Cauchy	$\ln(4\pi\gamma)$ (2.37)	γ: scale parameter
Chi-square	$\ln\left[2\Gamma\left(\frac{n}{2}\right)\right] + \left(1-\frac{n}{2}\right)\psi\left(\frac{n}{2}\right) + \frac{n}{2}$ (2.38)	n: positive integer

Differential entropy as a mathematical quantity finds wide utility in a number of important scientific disciplines (Michalowicz et al., 2013). For instance, in fluidization studies, Luckos et al. (2011) evaluated the Shannon's differential entropy in order to analyze the dynamics of gas-particle flow in a circulating fluidized bed. Additionally, both parameters, the Shannon and differential entropy, play important roles in information theory (Michalowicz et al., 2013) and authors such as Wang et al. (2017) and Luckos et al. (2011) described them as a promising technique and a good choice for characterizing the flow regimes in fluidized beds, respectively.

Moreover, analysing Table 2.5 and Table 2.6, it is noticed that not all parameters from the probability density functions influence the value of the differential entropy. For instance, take the Normal distribution. It needs two parameters for its characterization, the mean

(μ) and the variance (σ^2). The former is a location parameter and the latter is a scale parameter. Figure 2.7 is an example of Normal distributions with mean zero and different variances.

The mean of a Normal distribution corresponds to the point of symmetry. If it were different from zero, the graphics in Figure 2.7 would be shifted in the horizontal axis. On the other hand, the variance, or standard deviation (σ), is related to the dispersion of the distribution. It is important to mention that the fact that the differential entropy is directly related to the standard deviation is in accordance with the concept of uncertainty of the Shannon entropy, because the more possible events, the more choice, or uncertainty, there is. Small standard deviation implies a narrow distribution, while increasing values of standard deviation turns the distribution broader, and consequently, with more possible events.

Figure 2.7 – Examples of Normal distribution (adapted from Crooks, 2017).

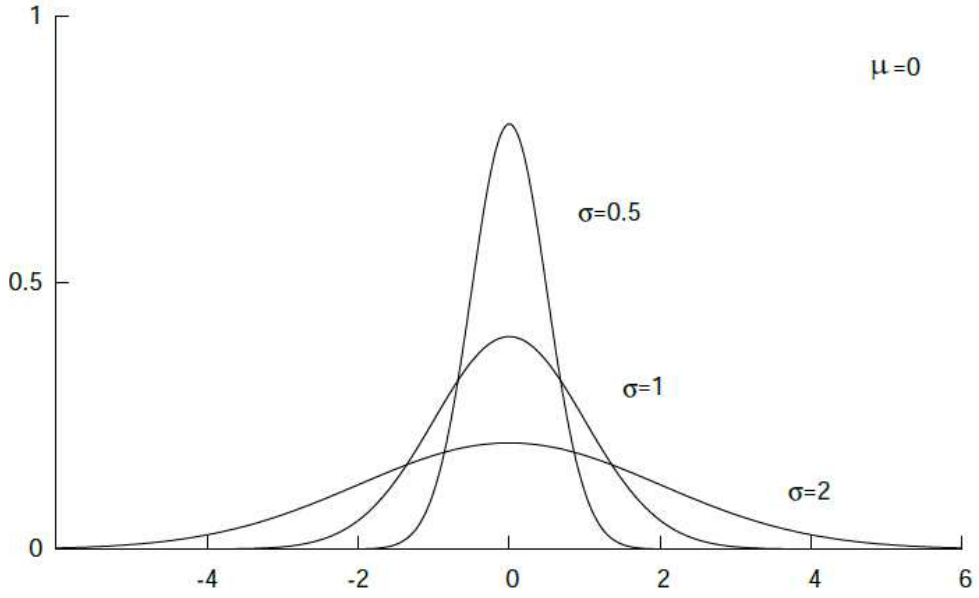

Coincidently, both parameters of the Normal distribution, the mean and the variance, are, in fact, the first and second moment, respectively, as it will be defined later. The average of a time series, for instance, was used to plot the fluidization curve. Table 2.1 showed several studies that used the second moment, in the form of standard deviation, to analyse the behavior of fluidization systems. Now, it is clear that, especially, the latter parameter is also associated with the differential entropy analysis.

Thus far, it has been discussed that to calculate the Shannon entropy, it would be necessary a frequency distribution. In order to transform a time series into a frequency distribution, the number of bins (n) that will group the data must be determined. The following

topic describes the method for the determination of *n* and introduces the concept of moments as well.

2.2.2 Determination of the number of bins

2.2.2.1 Moments

Mathematically, algebraic moments of order *r* are defined as the expectation value. If x_1, x_2, …, x_N are the *N* values assumed by the variable *x* (that is, *x(N)* can be a time series, for instance), the r^{th} moment is defined according to Equation 2.39 (Correa, 2003; Spiegel and Stephens, 2008).

$$\overline{x^r} = \frac{\sum x^r}{N} \tag{2.39}$$

Note that, when *r* equals 1, the first moment is defined as the arithmetic mean. Additionally, the r^{th} moment about the mean, also known as central moments of order *r*, follows Equation 2.40 (Spiegel and Stephens, 2008).

$$m_r = \frac{\sum(x - \bar{x})^r}{N} \tag{2.40}$$

The second central moment is the variance. As mentioned previously, the standard deviation is the square root of the variance, expressed in Equation 2.41.

$$\sigma = \sqrt{m_2} \tag{2.41}$$

The third and fourth central moments are used on the calculation of the coefficient of skewness (γ) and the coefficient of kurtosis (κ), respectively. The former is the degree of asymmetry of a distribution. If the frequency curve has a longer tail to the right of the central maximum than to the left, the distribution is said to have positive skewness, while the reverse is true and the distribution is then said to have negative skewness. The latter, on the other hand, is the degree of peakedness. A distribution having a relatively high peak is called leptokurtic and one which is flat-topped is called platykurtic. Both are usually taken relative to a normal

distribution, with γ_{normal} equals to zero and κ_{normal} equals to three, being called mesokurtic (Correa, 2003; Spiegel and Stephens, 2008). Equations 2.42 and 2.43 are the expressions for these parameters.

$$\gamma = \frac{m_3}{\sigma^3} \tag{2.42}$$

$$\kappa = \frac{m_4}{\sigma^4} \tag{2.43}$$

Although it is mathematically correct to calculate the moments of any series of points, the concept of degree of asymmetry and degree of peakedness, for instance, is clearer when it is referred to a frequency distribution, which is simply the arrangement of data by classes together with the corresponding class frequencies (Spiegel and Stephens, 2008). Figure 2.8 and Figure 2.9 are generic examples of frequency distributions with different coefficients of skewness and kurtosis, respectively.

Figure 2.8 – Example of asymmetric and symmetric distributions (adapted from Neckel, 2016).

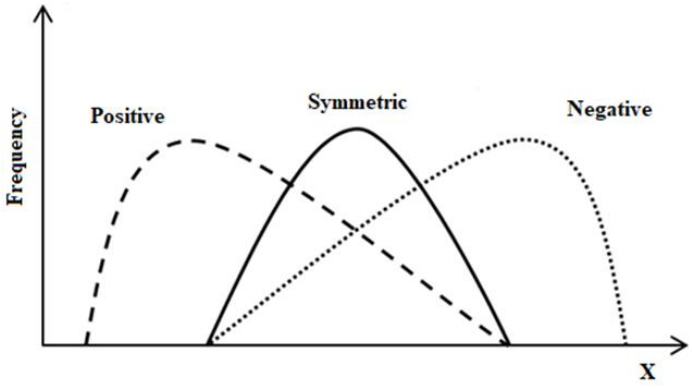

Figure 2.9 – Example of a leptokurtic, mesokurtic and platykurtic distribtutions (adapted from Neckel, 2016).

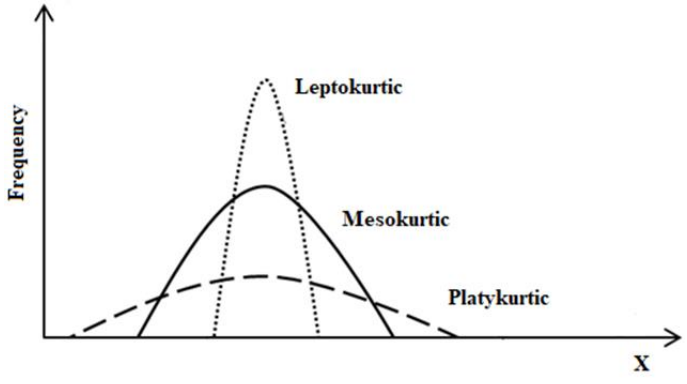

Additionally, pressure drop time series often exhibit asymmetric behavior, which, depending whether it is positive or negative asymmetry, affects the measures of central tendency, the arithmetic mean, the mode and the median.

The median of a set of numbers arranged in order of magnitude is either the middle value or the arithmetic mean of the two middle values. On the other hand, the mode of a set of numbers is that value which occurs with the greatest frequency, that is, the most common value (Spiegel and Stephens, 2008). Figure 2.10 and Figure 2.11 are generic asymmetric frequency distributions with their respective mean, mode and median indicated. Notice how, counterintuitively, the mean is not the most representative – the most frequent – value of a time series. Conversely, for a symmetrical distribution, like the normal distribution, the mean, the mode and the median coincide in the same value.

Figure 2.10 – Relative positions of mode, median and mean for a positive-skewed frequency distribution (adapted from Spiegel and Stephens, 2008).

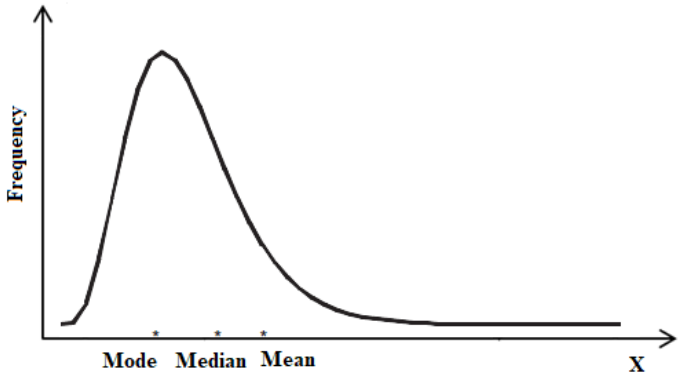

Figure 2.11 – Relative positions of mode, median and mean for a negative-skewed frequency distribution (adapted from Spiegel and Stephens, 2008).

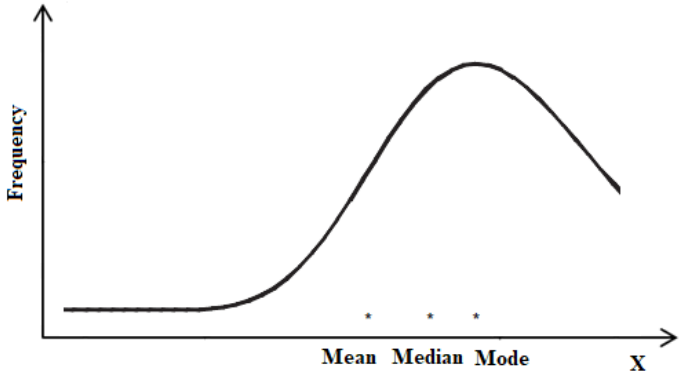

The ensuing topic will approach the method of the coefficient of variation in order to define an optimal number of class for each pressure drop time series and, eventually, calculate the Shannon entropy.

2.2.2.2 Method of the coefficient of variation

In order to transform a time series into a frequency distribution, it is necessary to determine the number of bins (n) that will group the data, as mentioned previously. There is a classical expression proposed by Sturges (1926), which depends on the total number of points (N) of the time series, according to Equation 2.44.

$$n = 1 + log_2 N \tag{2.44}$$

However, Sturges' rule does not consider the range, $x_{max} - x_{min}$, of the time series, which could underestimate the number of intervals for a large N. Scott (1979) studied the bin width of a distribution (Δ), taking into account the dispersion of the data points, in the form of standard deviation (σ), as well as the total number of points. The resultant expression is presented in Equation 2.45.

$$\Delta = \frac{3.49\sigma}{\sqrt[3]{N}} \tag{2.45}$$

The relation between Δ and n is expressed in Equation 2.46.

$$n = \frac{x_{max} - x_{min}}{\Delta} \tag{2.46}$$

If n is too large, there might be bins with null frequency, while if it is too small, there is loss of information. Moreover, the Shannon entropy is a monotonic increasing function of n. Thus, the selection of the number of bins is of primary concern for the Shannon entropy analysis. Therefore, instead of using Sturges' rule, which only depends on the total number of points, or Scott's rule, which tends to overestimate n, the coefficient of variation was used in this work to determine the number of bins.

The coefficient of variation (CV) is defined according to Equation 2.47 (Spiegel and Stephens, 2008).

$$CV = \frac{\sigma}{\bar{x}} \tag{2.47}$$

This parameter is the ratio of the standard deviation by the average of a frequency distribution. It is dimensionless and it calculates the relative dispersion of a distribution (Spiegel and Stephens, 2008).

The selection of the best bin consists in varying the number of bins and examine how the coefficient of variation, calculated from each distribution, evolves with the increase of bins. Figure 2.12 show an example of this method. The time series corresponds to the minimum fluidization point of the group B glass beads with 0.8 kg particle load, the same one presented in Figure 2.5.

First, the time series was transformed into a frequency distribution, and for each number of bin, the *CV* of that distribution was evaluated. Figure 2.12 is a plot of the evolution of the coefficient of variation with the number of bins.

The number of bins is obtained from the intersection of the two straight lines depicted in the plot. It is worth mentioning that this graphic is an adaptation of the plot found in Prieto et al. (2017.a), who evaluated the number of bins for minimum fluidization pressure drop time series using the same method. Hence, the number of bins that would be selected is 26.

Figure 2.12 – Evolution of the coefficient of variation for the time series of the minimum fluidization point of group B glass beads with 0.8 kg particle load (adapted from Prieto et al., 2017.a).

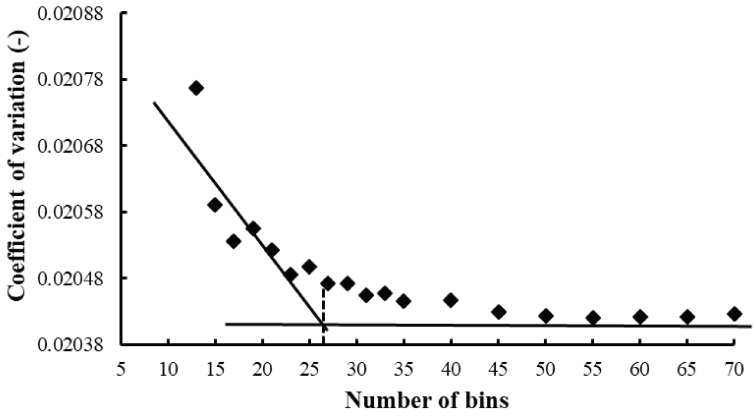

Figure 2.13 is the frequency distribution of the time series for the minimum fluidization point of group B glass beads with 0.8 kg particle load with the number of bins, or classes, being equal to 26.

Figure 2.13 – Frequency distribution for the minimum fluidization point of group B glass beads with 0.8 kg particle load (n = 26).

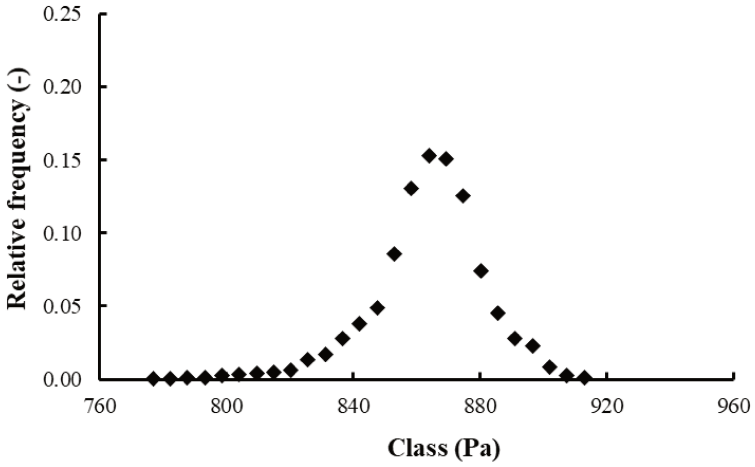

Until this point, it has been discussed that, for the calculation of the differential entropy, the model with the smallest difference from the experimental data will be the elected probability density function. However, there is also the need of determining a critical value, which would be the maximum difference allowed between the experimental data and the model in order to not reject the hypothesis that the data do fit the assumed distribution. Thus, the method used in this Dissertation for testing the goodness of fit is the Kolmogorov-Smirnov test. It is a reliable and commonly used test and has the advantage of having a straightforward procedure (O'Connor and Kleyner, 2012).

2.2.2.3 Kolmogorov-Smirnov test

The Kolmogorov-Smirnov (K-S) is a nonparametric test. It compares the cumulative distribution $F(x)$ of a PDF with the corresponding experimental cumulative distribution $S(x)$. The procedure of the Kolmogorov-Smirnov test is (Bohm and Zech, 2010; O'Connor and Kleyner, 2012):

- Calculate the values of $|F(x_i) - S(x_i)|$ where $F(x_i)$ is the i^{th} cumulative value and $S(x_i)$ the expected cumulative value for the assumed distribution.
- Determine the highest single value.
- Compare this value with the appropriate K-S critical value.

Figure 2.14 shows a comparison of a fictional empirical distribution with the theoretical one.

Figure 2.14 – Example of a Kolmogorov-Smirnov test (Bohm and Zech, 2010).

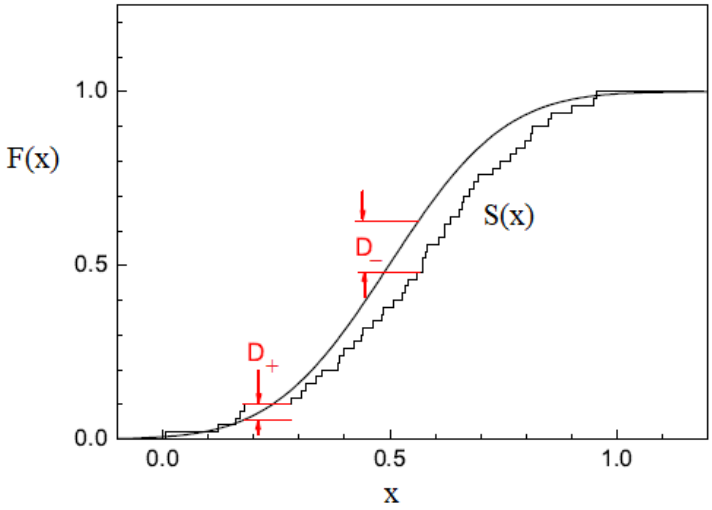

where D_+ and D_- are the maximum positive and negative difference, respectively. Mathematically, the quantity D is defined according to Equation 2.48.

$$D = sup|F(x) - S(x)| \tag{2.48}$$

There is a critical value for D that will either accept or reject the hypothesis that the theoretical distribution function can represent the experimental data. This value, D_c, depends on the numbers of bins that the series is divided into. They are usually presented in form of tables, such as Table 2.7 according to the level of significance.

Table 2.7 – Critical values for the Kolmogorov-Smirnov test (adapted from O'Connor and Kleyner, 2012).

Number of bins (n)	**Level of significance (%)**			
	10	5	2	1
18	0.27851	0.30936	0.34569	0.37062
19	0.27136	0.30143	0.33685	0.36117
20	0.26473	0.29408	0.32866	0.35241
21	0.25858	0.28724	0.32104	0.34427
22	0.25283	0.28087	0.31394	0.33666

Table continued

23	0.24746	0.27490	0.30728	0.32954
24	0.24242	0.26931	0.30104	0.32286
25	0.23768	0.26404	0.29516	0.31657
26	0.23320	0.25907	0.28692	0.31064
27	0.22898	0.25438	0.28438	0.30502
28	0.22497	0.24993	0.27942	0.29971
29	0.22117	0.24571	0.27471	0.29466
30	0.21756	0.24170	0.27023	0.28987
31	0.21412	0.23788	0.26596	0.28530
32	0.21085	0.23424	0.26189	0.28094
33	0.20771	0.23076	0.25801	0.27677
34	0.20472	0.22743	0.25429	0.27279
35	0.20185	0.22425	0.26073	0.26897
36	0.19910	0.22119	0.24732	0.26532
37	0.19646	0.21826	0.24404	0.26180
38	0.19392	0.21544	0.24089	0.25843
39	0.19148	0.21273	0.23786	0.25518
40	0.18913	0.21012	0.23494	0.25205

The level of significance chosen for this Dissertation is 5%, a conventional value as the critical level of significance (Tippet, 1951). If D is greater than D_c, the hypothesis is rejected, that is, the theoretical distribution is not a good fit for the experimental data.

For n greater than 40 and a level of significance of 5%, D_c can be estimated by Equation 2.49 (O'Connor and Kleyner, 2012).

$$D_c = \frac{1.36}{\sqrt{n}} \tag{2.49}$$

3. METHODOLOGY

3.1 Materials

The pressure time series analysed in this work were experimentally obtained by Prieto (2014), who worked with gas-particle fluidization. The experiments were performed at the Laboratory of Processes in Porous Media, at School of Chemical Engineering, University of Campinas. Table 3.1 shows the characteristics of the particulate phases.

Table 3.1 – Properties of the particulate phase (Prieto, 2014).

Material	Density (kg/m^3)	Average diameter (μm)	Geldart classification
glass bead	2,500	64	A
glass bead	2,500	128	B
glass bead	2,500	1200	D

The total particle loads in the bed were 0.4 and 0.8 kg and the fluid phase was atmospheric air, at 25 ºC (ρ_{air} = 1.184 kg/m^3).

The experimental apparatus used in this work is presented in Figure 3.1. Point A is the column, made of acrylic with an inside diameter and height of 10 and 100 cm, respectively; B indicates the Lapple cyclone, which would collect any material eventually dragged; C points out the distribution plate, with 0.27 cm orifices spaced in a 0.75 cm triangular pattern; and D is the panel where the data acquisition system was installed. It contained two sealed 12 V batteries with the purpose of eliminate noise from the electrical grid. The whole structure is mounted on a metallic support. Figure 3.2 displays the dimensions and configuration of the distribution plate (a), the Lapple cyclone (b) and the fluidized bed (c). Additionally, a 400 mesh screen was used with the distribution plate in order to retain the fine particles (Prieto, 2014).

The blower which was used to provide air to the system was located outside the laboratory. It has a maximum flow of 3.9 m^3/min and pressure of 3,600 mmwc. The discharge tube has 40 cm pipe length and 10 cm internal diameter and is made of rubber. It is connected to a 70 cm stainless steel tube, with a square elbow, a ball valve (fully open), a by-pass controlled by a globe valve (fully closed) and a reducer. The remainder of the pipe is made of PVC with a length of 190 cm and nominal diameter of 1.5 inches.

Figure 3.1 – Experimental apparatus for the gas-particle fluidization (Prieto, 2014).

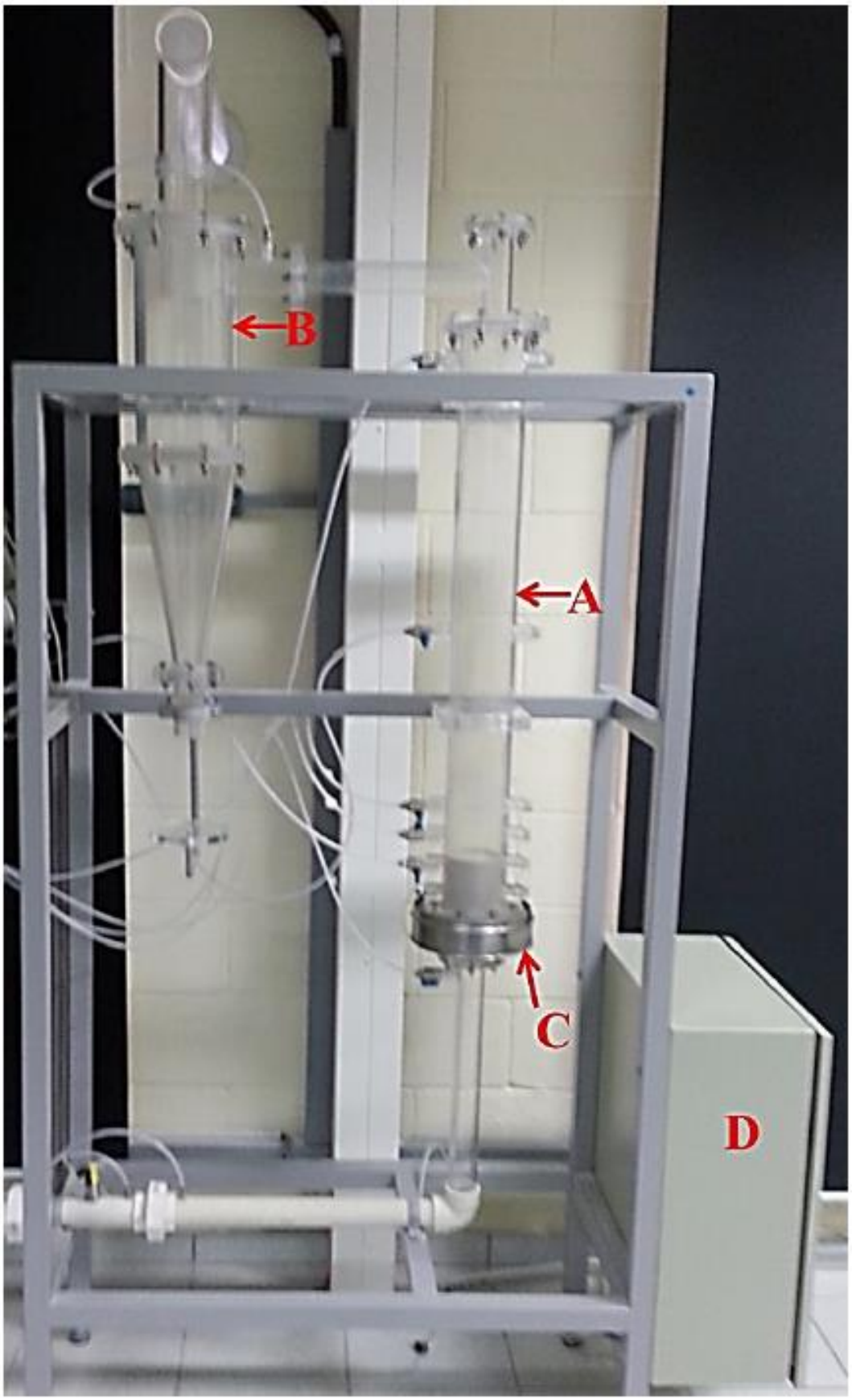

Figure 3.2 – Dimensions and configurations of the distribution plate, Lapple cyclone and fluidized bed (Prieto, 2014).

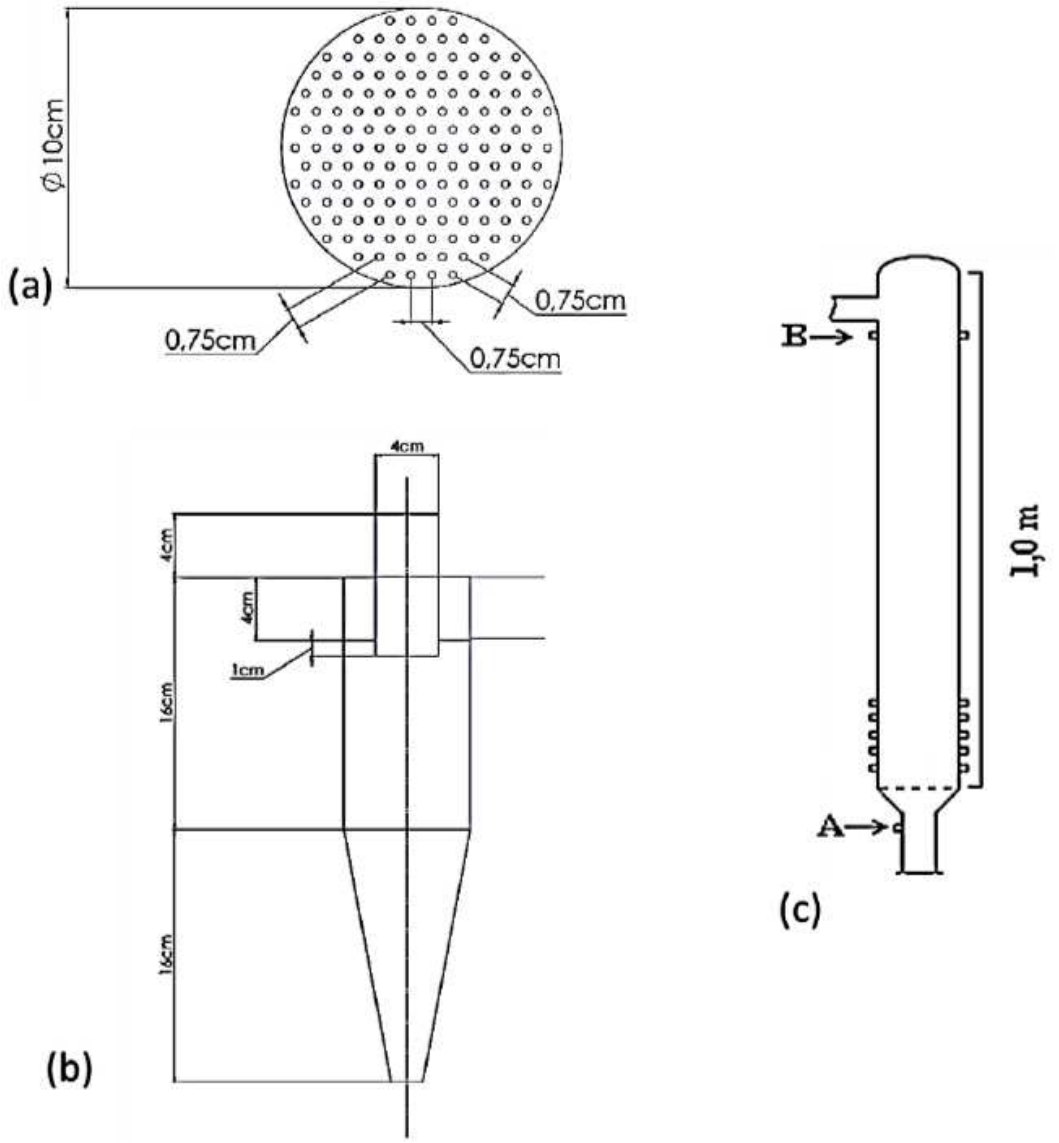

The data acquisition system consists of differential and absolute pressure transducers and a temperature sensor. For the pressure drop in the bed, it was used differential pressure transducer fabricated by *NOVUS*, model *NP800H*. They were positioned before the distribution plate and at the exit of the column, as it is shown in Figure 3.2(c) (points A and B). To determine the air flow, it was used an orifice plate, made of stainless steel, with its pressure drop being measured by a differential pressure transducer, also fabricated by *NOVUS*, model *NP800H*. The air temperature and absolute pressure were obtained, respectively, by a temperature sensor, *INCON Pt100 3F*, 5 cm before the orifice plate, and an absolute pressure transducer *NOVUS NP430D*, before the plate.

The acquisition frequency and sample time, for all experiments, were 1,000 Hz and 40 s, respectively. The acquisition system has an Analog to Digital Converter (ADC) resolution of 16 bits. In order to mitigate the effect of noise, it was implemented in the data acquisition system a low pass filter with infinite impulse response (IIR), with 25th order Butterworth topology (Prieto, 2014).

The operating system used in this work was *Windows 10 Home* 64 *bits*, *Intel Core i7* processor with 8GB of RAM and the software used for the analysis were *Microsoft Office Excel 2013* 32-*bit*. The programming language, *VBA* (*Visual Basic for Applications*) of the *Excel* was chosen because it is highly diffunded in the world. Moreover, it has functions in their internal packages to help in the signal processing.

3.2 Methods

Figure 3.3 shows a flowchart for the Shannon entropy analysis.

Starting with the experimental time series, the moments are calculated for each one of them. The first moment, which is the arithmetic mean, can be used to construct the fluidization curve and identify regimes, for instance. Another analysis that is part of the method of moments is the evaluation of the amplitude of the signals, through the standard deviation. This latter parameter has been extensively employed in the Literature in the analysis of pressure drop time series of a fluidized bed.

Alternatively, in order to calculate the Shannon entropy, it is necessary to transform the time series into a frequency distribution. Consequently, the numbers of bins (n) must be determined. However, if n is too large, there might be bins with null frequency, while if it is too small, there is loss of information. Therefore, the number of bins was calculated via the method of the coefficient of variation (CV). The value of n adopted was obtained from the intersection of the two straight lines depicted in the plot of the evolution of CV versus n (such as in the example in Figure 2.12). This same methodology has been used before and can be found in Prieto et al. (2017.a).

Once all data were analysed via the method of the coefficient of variation, the number of bins was determined individually for each time series. Then, the frequency distribution created is now used to determine the Shannon entropy by approximating the relative frequency of a given class to the probability of it occurring and using Equation 2.6. Subsequently, it was used as the experimental distribution in the Kolmogorov-Smirnov test.

The theoretical distributions presented in Table 2.5 were modelled to fit the experimental one. The theoretical distribution selected was the one that presents the smaller sum of squared errors and that passes the K-S test. The level of significance chosen was 5%, a conventional value as the critical level of significance (Tippet, 1951). Thus, with the theoretical PDF selected and its parameters calculated, the differential Shannon entropy was evaluated. The Shannon and the differential Shannon entropy are compared. Finally, the Shannon entropy was used to identify the fluidization regimes.

Figure 3.3 – Flowchart for the calculation of the Shannon entropy.

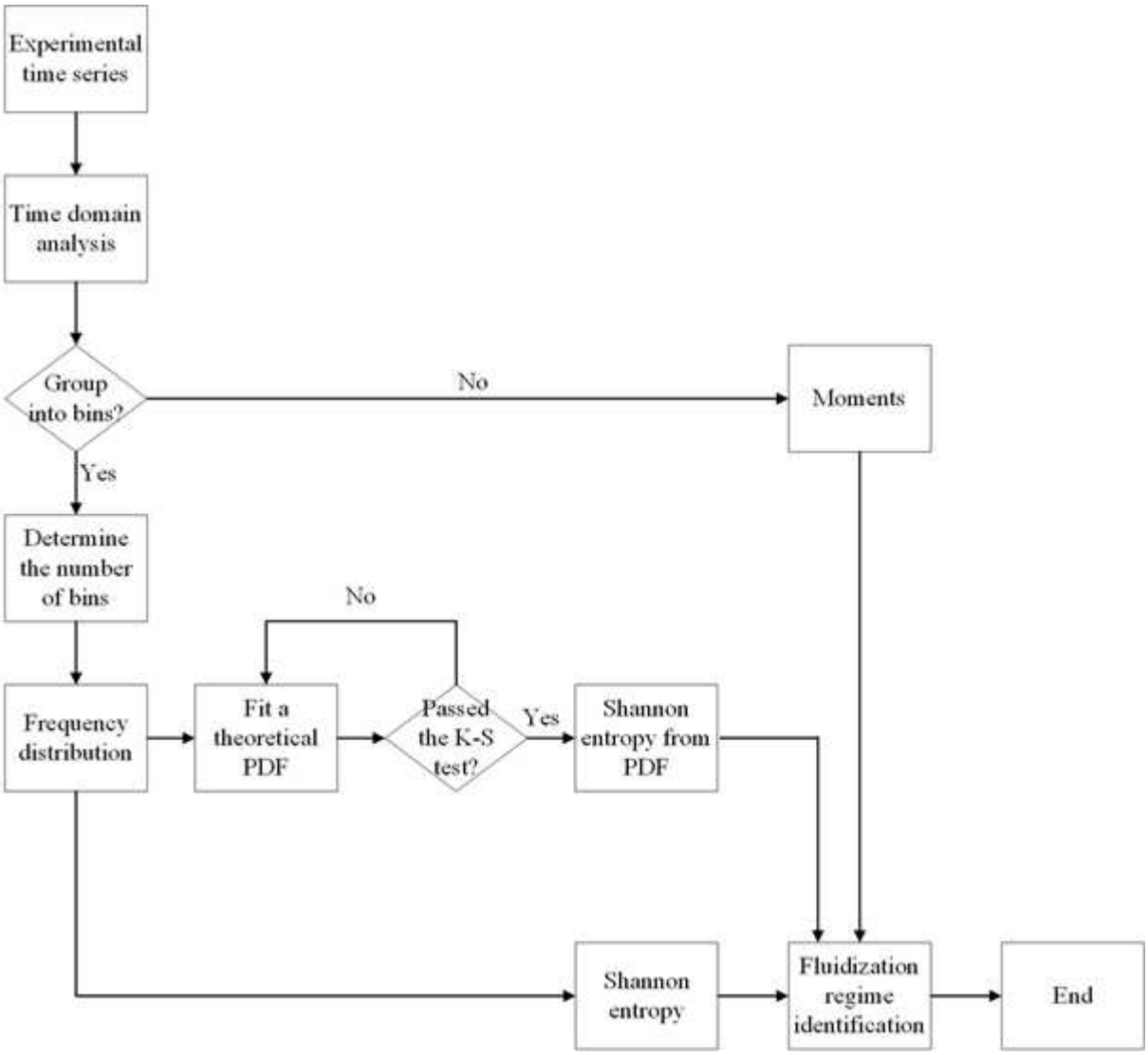

4. RESULTS AND DISCUSSION

This topic analyzes the fluidization of the particulate phase presented in section 3. Firstly, the average of the time series was used to construct the fluidization curve and characterize the regimes. Then, the number of bins was determined in order to create the frequency distribution for each time series. Next, once each histogram was established, the Shannon entropy is evaluated and the theoretical probability density functions were fitted into the experimental data.

4.1 Fluidization curve

Starting with the group A from the Geldart classification, Figure 4.1 shows the fluidization curve for a total particle load in the bed of 0.4 and 0.8 kg. Each point in the plots corresponds to the average value of the 40,000 points experimental time series. The vertical lines that separate the regions (I), (II) and (III) are the velocities where a regime transition have occurred, as it was identified by direct observation of the bed by Prieto (2014). The minimum fluidization velocity and pressure drop for the 0.4 and 0.8 kg particle load are U_{mf} = 0.24 m/s and ΔP_{mf} = 602 Pa and U_{mf} = 0.25 m/s and ΔP_{mf} = 773 Pa, respectively.

It is worth mentioning that the fluidization curves were obtained with decreasing velocity and the minimum fluidization point is also obtained from the intersection of two straight lines depicted in the experimental curves.

The particulate, or expanded bed, regime (I) displays a linear increase in the pressure drop with increasing gas velocity. In this region, the weight of the bed overcomes the frictional drag force, causing the fluid to only percolate the particles, which remain motionless. As the minimum fluidization velocity is approached, the movement in the bed intensifies, altering the bed voidage. After the minimum fluidization point, it was noticed the formation of bubbles, characterizing, then, the bubbling regime (region (II)). The last one exhibits a raise on the pressure drop, above the minimum fluidization point, representing the slug flow regime. The transitions from bubbling to slug flow regime are given by U/U_{mf} equals to 1.15 and 1.17 for the particle loads of 0.4 and 0.8 kg, respectively.

The small diameter of the Geldart A glass beads soothes the pressure drop variation, as the gas velocity increases. This is reflected on the gradual slope of the fluidization curves. The quick transition of the bubbling bed to the slug flow regime is another consequence of the

particulate phase properties. Additionally, the heavier bed needs a higher velocity in order to fluidize, as it was expected, since the resistance to the air flow is proportional to the particle load. The pressure drop curves, in Figure 4.1, clearly captured the minimum fluidization point, while they could not distinguish the transition between bubbling and slug flow regimes.

Figure 4.1 – Average pressure drop versus the normalized gas velocity in the fluidization of Geldart A particles – particle load of (a) 0.4 kg and (b) 0.8 kg.

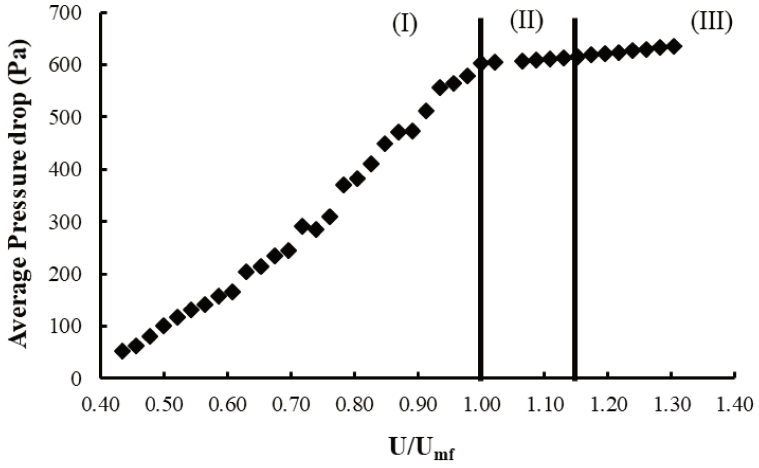

(a)

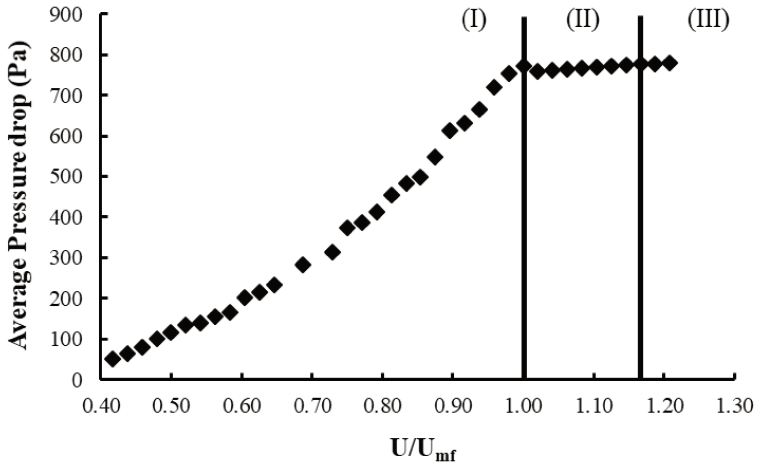

(b)

Likewise in the case of the Geldart A particles, Figure 4.2 gives the fluidization curves for the glass beads belonging to the B group. Moreover, the minimum fluidization velocity and pressure drop for the 0.4 and 0.8 kg particle load are, respectively, U_{mf} = 0.26 m/s and ΔP_{mf} = 485 Pa and U_{mf} = 0.28 m/s and ΔP_{mf} = 864 Pa. Again, the vertical lines separate the particulate (I), the bubbling bed (II) and the slug flow regime (III), which were also visually

identified by Prieto (2014). The transitions from bubbling to slug flow regime are given by U/U_{mf} equals to 3.06 and 3.23 for the particle loads of 0.4 and 0.8 kg, respectively.

Figure 4.2 – Average pressure drop versus the normalized gas velocity in the fluidization of Geldart B particles – particle load of (a) 0.4 kg and (b) 0.8 kg.

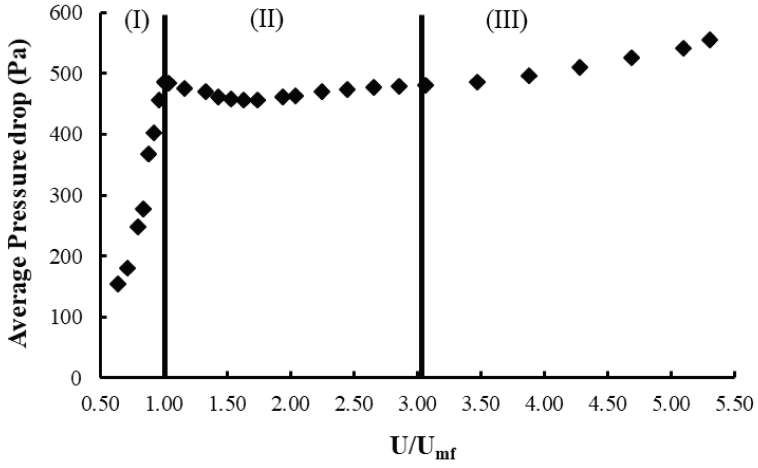

(a)

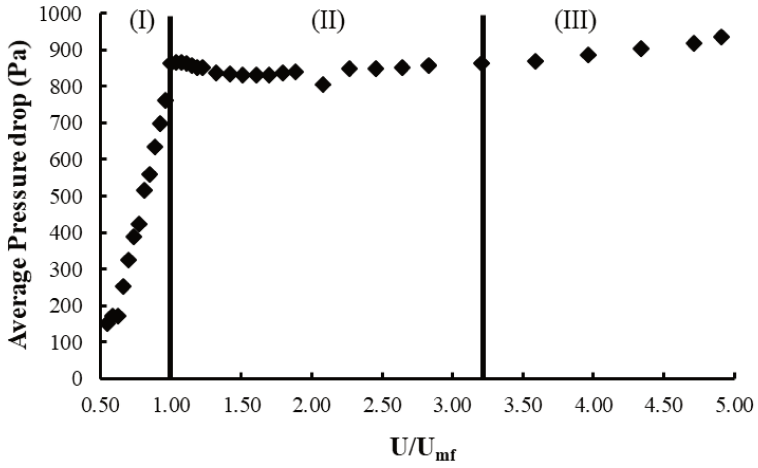

(b)

Similarly to the glass beads from group A, the particulate regime, region (I), also has a linear increase pressure drop with increasing gas velocity, but with a steeper slope. The difference between the fluidization curves in Figure 4.2 is due to the particle load in the bed. For the lighter case, lower air velocities were necessary for the two regime transitions. Moreover, as it is expected of the Geldart B particles, they readily bubble at the minimum fluidization velocity. After the transition to the slug flow regime, there is a raise in the pressure drop as well.

Lastly, Figure 4.3 presents the fluidization curves for the Geldart D glass beads for the particle loads of 0.4 and 0.8 kg. The minimum fluidization velocity and pressure drop are U_{mf} = 0.65 m/s and ΔP_{mf} = 2,340 Pa and U_{mf} = 0.80 m/s and ΔP_{mf} = 3,367 Pa, in that order. The vertical lines separate the regimes identified by Prieto (2014), which are the same ones of the A and B particles, the particulate (I), the bubbling bed (II) and the slug flow regime (III). The transitions to slug flow regime are given by U/U_{mf} equals to 1.42 and 1.47 for both particle loads, respectively.

Figure 4.3 – Average pressure drop versus the normalized gas velocity in the fluidization of Geldart D particles – particle load of (a) 0.4 kg and (b) 0.8 kg.

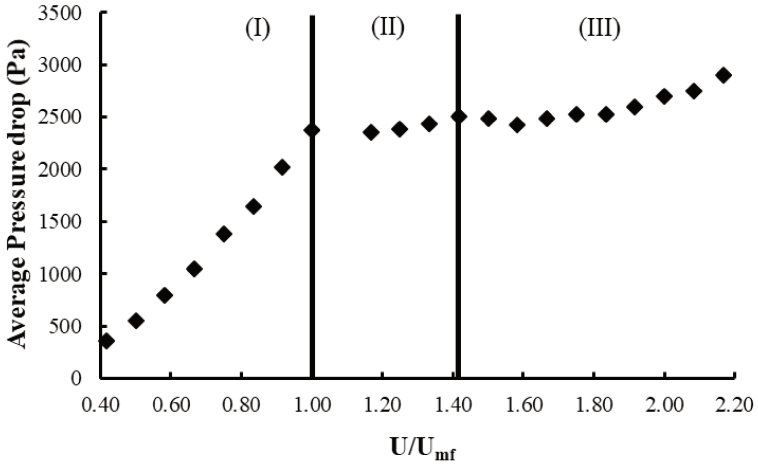

(a)

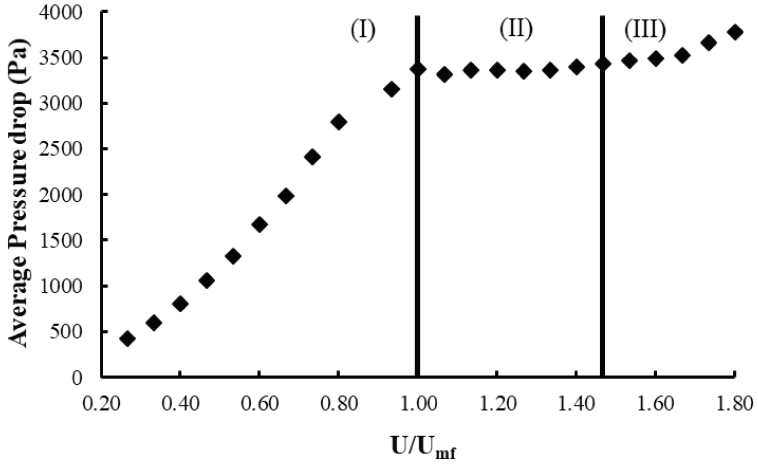

(b)

The fluidization curves of the Geldart D particles displayed similar development to the plots of A and B glass beads. It is important to mention that Prieto (2014) also observed the formation of some bubbles at velocities lower than the minimum fluidization point, which is

worth remembering, were determined by analysing the plot of pressure drop versus superficial gas velocity. They have begun forming at U/U_{mf} equal to 0.50 and 0.67 for the particle loads of 0.4 and 0.8 kg, respectively, and eventually evolved to the bubbling and slug flow regime for higher velocities. Moreover, particles from the group D of the Geldart classification fluidize better in a spouted bed. Prieto (2014), who performed the experiments, justifies the use of a fluidized bed in order to be able to compare the results of the particles A and B in the same base.

The next topic demonstrates how the number of bins was determined for each time series.

4.2 Determination of the number of bins

The determination of the number of bins (n) is an important step for the further analysis of Shannon entropy. As mentioned previously, in a frequency distribution, the data is arranged by classes together with the corresponding class frequencies. Then, each class is defined by the average value of its lower and upper limit. Therefore, n cannot be too small, which would implicate in the loss of information, nor too large, which would create classes with null frequency.

The Sturges' rule depends only on the time series total number of points. Since all of them have 40,000 points, the number of bins calculated by Sturges' rule is 17. On the other hand, Scott's rule takes into account the dispersion of the data points, through the standard deviation, as well as the total number of points. This latter rule tends to overestimate the number of bins. The results found varied from 40 to 113. Since the Shannon entropy is monotonically increasing with n, the method adopted for the determination of the number of bins is the coefficient of variation.

Similarly to the example presented in section 2.4.2 for the minimum fluidization time series for the 0.8 kg Geldart B particles, Figure 4.4 displays the evolution of the coefficient of variation with the number of bins for the B glass beads with 0.8 kg particle load. The time series were purposely selected from different fluidization states, that is, the particulate regime (a), minimum fluidization point (b), bubbling (c) and slug flow regime (d). Hence, the number of bins, obtained from the intersection of the two straight lines depicted in the plots, to group each of these time series are 22, 26, 23 and 21, respectively.

Figure 4.4 – Evolution of the coefficient of variation for the fluidization of 0.8 kg of Geldart B glass beads – (a) $U/U_{mf} = 0.92$, (b) $U/U_{mf} = 1.00$, (c) $U/U_{mf} = 2.45$ and (d) $U/U_{mf} = 4.34$.

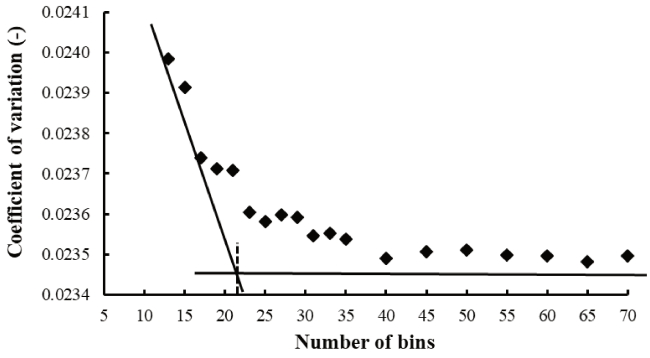

(a)

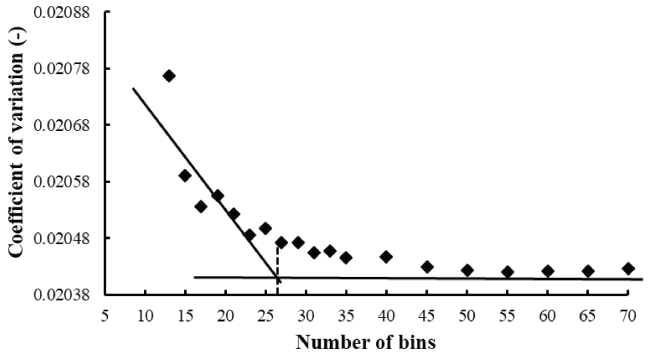

(b)

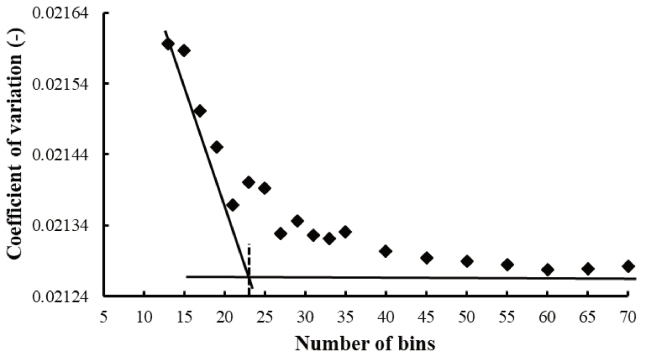

(c)

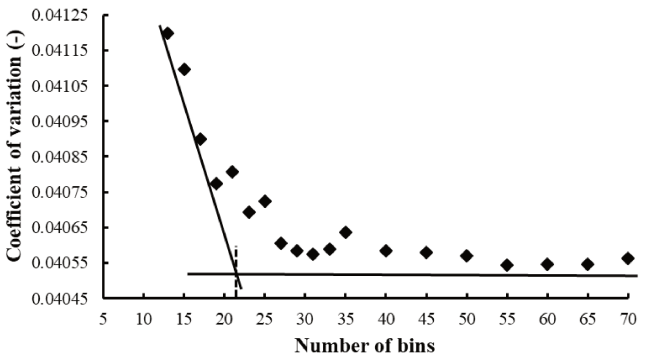

(d)

Figure 4.5 presents the transformation the four time series of Figure 4.4 into frequency distributions with their respective number of bins.

Figure 4.5 – Transformation of time series into frequency distribution for the fluidization of 0.8 kg of Geldart B glass beads – (a) $U/U_{mf} = 0.92$, (b) $U/U_{mf} = 1.00$, (c) $U/U_{mf} = 2.45$ and (d) $U/U_{mf} = 4.34$.

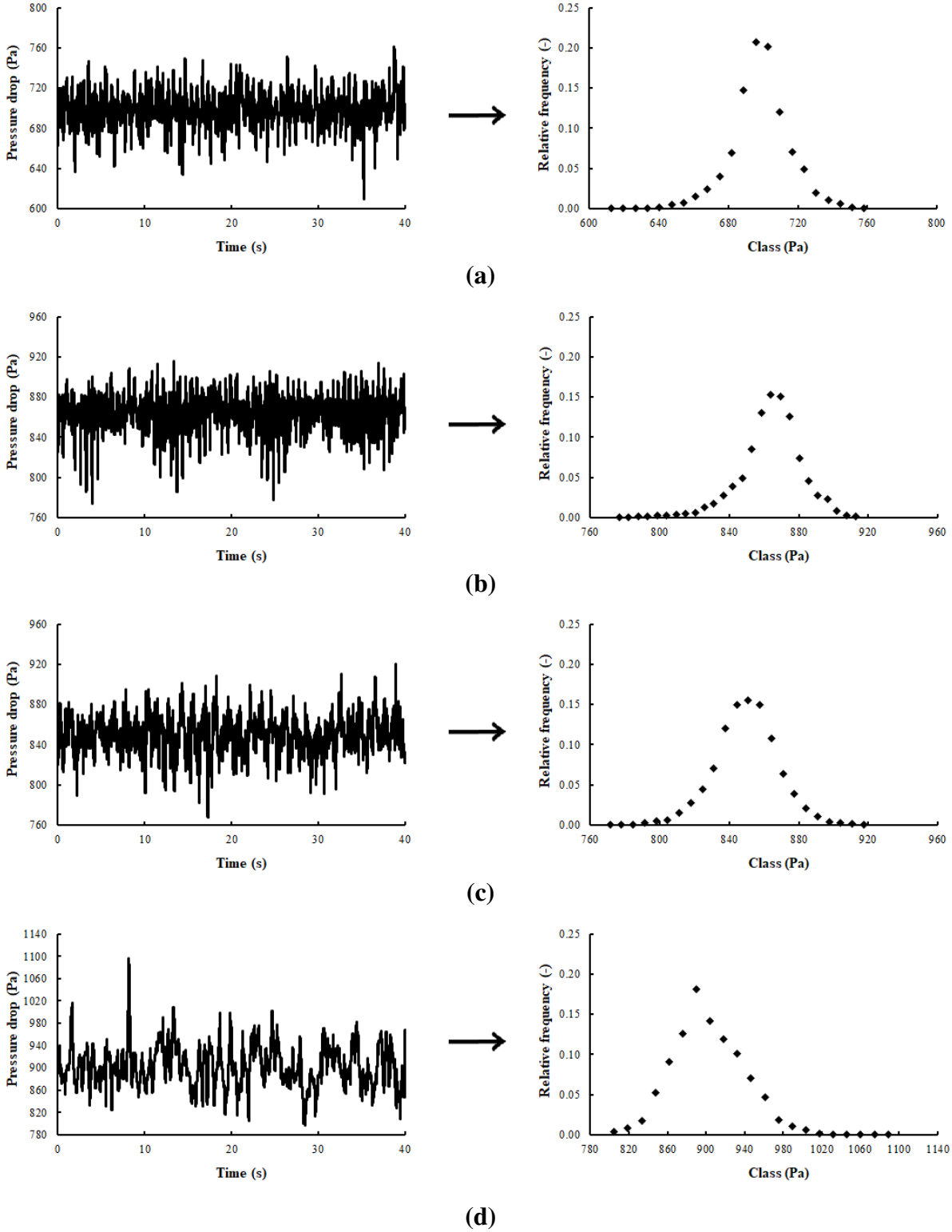

Notice how time series from different regimes are visually distinct when simply analysed in a time plot. Consequently, the resultant frequency distribution also show this contrast. The concept of the coefficient of skewness and kurtosis become more understandable now. For lower velocities, the frequency distributions seem to be skewed to the left (negative asymmetry) and they are not as broad as the ones from the bubbling and slug flow regime. This latter characteristic is directly related to the standard deviation. Table 4.1 shows the number of bins determined by this same methodology for every time series in the fluidization of 0.4 kg A glass beads.

Table 4.1 – Number of bins determined by the method of the coefficient of variation for the 0.4 kg A glass beads.

U/U_{mf}	n	U/U_{mf}	n
0.4348	19	0.8696	24
0.4565	22	0.8913	25
0.4783	20	0.9130	20
0.5000	19	0.9348	26
0.5217	24	0.9565	27
0.5435	20	0.9783	27
0.5652	23	1.0000	27
0.5870	20	1.0217	29
0.6087	19	1.0652	20
0.6304	26	1.0870	22
0.6522	25	1.1087	22
0.6739	24	1.1304	20
0.6957	23	1.1522	20
0.7174	24	1.1739	19
0.7391	21	1.1957	19
0.7609	19	1.2174	24
0.7826	24	1.2391	21
0.8043	24	1.2609	19
0.8261	23	1.2826	19
0.8478	25	1.3043	19

Analogously, Table 4.2 continues the analysis of the number of bins for the fluidization of A glass beads, but this time for a particle load of 0.8 kg.

Table 4.2 – Number of bins determined by the method of the coefficient of variation for the 0.8 kg A glass beads.

U/U_{mf}	n	U/U_{mf}	n
0.4167	25	0.8542	21
0.4375	20	0.8750	25
0.4583	24	0.8958	22
0.4792	25	0.9167	23
0.5000	20	0.9375	22
0.5208	20	0.9583	24
0.5417	24	0.9792	25
0.5625	28	1.0000	26
0.5833	20	1.0208	20
0.6042	28	1.0417	28
0.6250	28	1.0625	20
0.6458	28	1.0833	23
0.6875	28	1.1042	26
0.7292	22	1.1250	20
0.7500	25	1.1458	21
0.7708	21	1.1667	22
0.7917	22	1.1875	20
0.8125	22	1.2083	20
0.8333	26	-	-

The shape of the frequency distribution will influence the calculation of the Shannon entropy. For instance, if a distribution presents asymmetry, it will have a longer tail to the right or to the left (positive or negative asymmetry, respectively). Moreover, the fact that a distribution is leptokurtic or platykurtic will also affect the Shannon entropy. In a leptokurtic distribution, the center peak is high and the probabilities are concentrated in a narrow range of classes while in a platykurtic distribution the probabilities of the classes are more uniform as the distribution presents a flatter and broader feature than the former one. Consequently,

depending on the shape of the frequency distribution, there can be less or more classes with small probabilities, such as the classes that are part of the tails.

Since the Shannon entropy is the summation of the product of the probability and its logarithm, the fact that different regimes have different frequency distributions, as exemplified in Figure 4.5, it is logical to infer that this parameter can be used to identify and differentiate fluidization states.

Additionally, proceeding with the analysis, Table 4.3 presents the number of bins for the fluidization of 0.4 kg B glass beads.

Table 4.3 – Number of bins determined by the method of the coefficient of variation for the 0.4 kg B glass beads.

U/U_{mf}	n	U/U_{mf}	n
0.6327	25	1.7347	24
0.7143	21	1.9388	21
0.7959	22	2.0408	22
0.8367	23	2.2449	22
0.8776	24	2.4490	22
0.9184	22	2.6531	26
0.9592	25	2.8571	21
1.0000	25	3.0612	20
1.0408	25	3.4694	21
1.1633	24	3.8776	23
1.3265	24	4.2857	25
1.4286	21	4.6939	22
1.5306	22	5.1020	19
1.6327	23	5.3061	20

It is important to remember that the number of bins determined for each time series so far is not constant, as it would be if it was to be calculated by the Sturges' rule. Also, the number of bins obtained by the method of the coefficient of variation does not vary as much as the ones calculated by the Scott's rule. As mentioned previously, the individual optimization of the number of classes that will group each time series is an important step in the Shannon entropy analysis due the fact that one of the properties inherent of this parameter, the one that

says if all probabilities are equal, and *n* is the number of possible events, that is, *n* is the number of bins, then the Shannon entropy should be a monotonic increasing function of *n*. This means that with equally likely events there is more choice, or uncertainty, when there are more possible events.

Table 4.4 displays the number of bins for the case of 0.8 kg particle load of the fluidization of B glass beads.

Table 4.4 – Number of bins determined by the method of the coefficient of variation for the 0.8 kg B glass beads.

U/U_{mf}	n	U/U_{mf}	n
0.5472	21	1.3208	26
0.5849	25	1.4151	24
0.6226	22	1.5094	24
0.6604	20	1.6038	25
0.6981	21	1.6981	25
0.7358	20	1.7925	25
0.7736	21	1.8868	20
0.8113	21	2.0755	23
0.8491	24	2.2642	20
0.8868	22	2.4528	23
0.9245	22	2.6415	22
0.9623	20	2.8302	22
1.0000	26	3.2075	20
1.0377	20	3.5849	20
1.0755	23	3.9623	19
1.1132	24	4.3396	21
1.1509	24	4.7170	20
1.1887	25	4.9057	19
1.2264	25	-	-

Lastly, Table 4.5 and Table 4.6 are the number of bins for the D glass beads for the cases of 0.4 and 0.8 kg total particle load, respectively.

Table 4.5 – Number of bins determined by the method of the coefficient of variation for the 0.4 kg D glass beads.

U/U_{mf}	n	U/U_{mf}	n
0.4167	20	1.4167	24
0.5000	22	1.5000	24
0.5833	23	1.5833	24
0.6667	20	1.6667	21
0.7500	27	1.7500	22
0.8333	25	1.8333	26
0.9167	26	1.9167	26
1.0000	26	2.0000	27
1.1667	23	2.0833	21
1.2500	25	2.1667	20
1.3333	22	-	-

Table 4.6 – Number of bins determined by the method of the coefficient of variation for the 0.8 kg D glass beads.

U/U_{mf}	n	U/U_{mf}	n
0.2667	24	1.1333	24
0.3333	21	1.2000	21
0.4000	24	1.2667	28
0.4667	22	1.3333	26
0.5333	22	1.4000	23
0.6000	25	1.4667	23
0.6667	24	1.5333	24
0.7333	24	1.6000	20
0.8000	22	1.6667	21
0.9333	25	1.7333	20
1.0000	25	1.8000	19
1.0667	24	-	-

Therefore, since the number of bins for all time series is determined, the Shannon entropy can be evaluated, which is the subject of the ensuing topic.

4.3 Shannon entropy

The Shannon entropy quantifies the average unpredictability in a random variable and, as it was mentioned previously, it can be associated with the complexity of particulate systems. Hence, Figure 4.6, Figure 4.7 and Figure 4.8 are the Shannon entropy versus the normalized gas velocity for the fluidization of the three types of particles for the particle loads of 0.4 and 0.8 kg. All of those plots were constructed using the number of bins determined in section 4.2. The vertical lines that separate the regions (I), (II) and (III) are the same velocities where a regime transition have occurred, as it was also identified in the fluidization curves in section 4.1.

Figure 4.6 – Shannon entropy versus the normalized gas velocity in the fluidization of Geldart A particles – particle load of (a) 0.4 kg and (b) 0.8 kg.

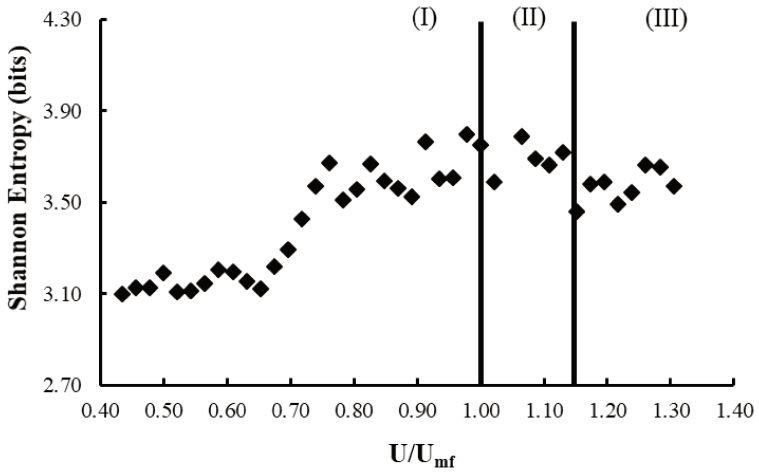

(a)

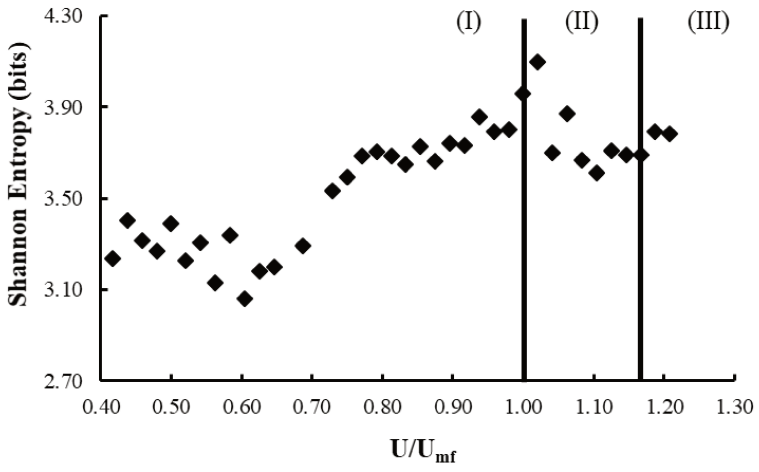

(b)

Figure 4.7 – Shannon entropy versus the normalized gas velocity in the fluidization of Geldart B particles – particle load of (a) 0.4 kg and (b) 0.8 kg.

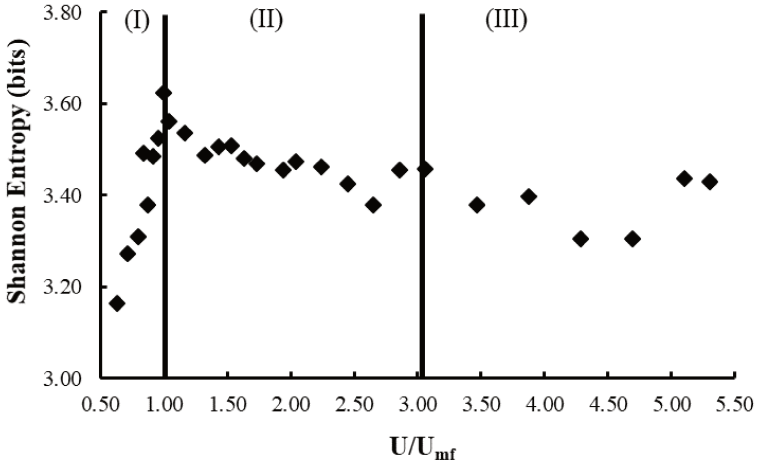

(a)

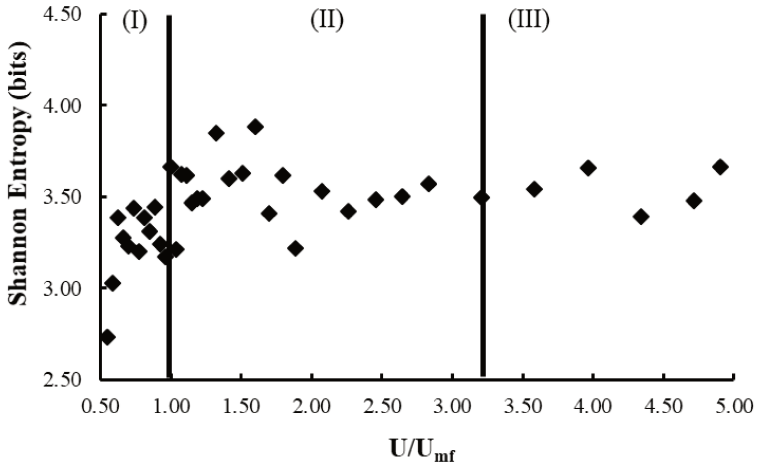

(b)

Firstly, it is noticed that positive *H* were obtained even for velocities below the minimum fluidization point for all cases. This result means that it is not possible to absolutely be able to predict the pressure drop time series and it is in accordance with what Prieto (2014) obtained, positive values of Kolmogorov entropy for all time series as well.

The overall trend is that the Shannon entropy remains low at low velocities, then, it continuously increases until reaching a maximum in the region around the minimum fluidization point and finally drops slightly. Moreover, for velocities beyond the transition of the bubbling to slug flow regime, the Shannon entropy seemed to, generally, present an increasing pattern as well.

Figure 4.8 – Shannon entropy versus the normalized gas velocity in the fluidization of Geldart D particles – particle load of (a) 0.4 kg and (b) 0.8 kg.

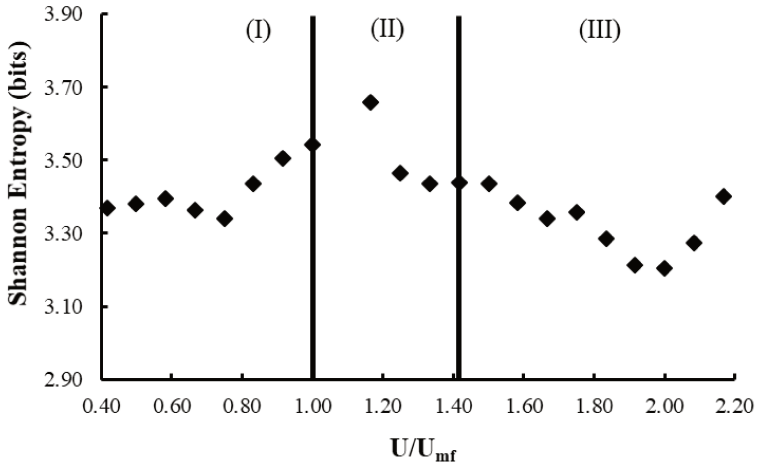

(a)

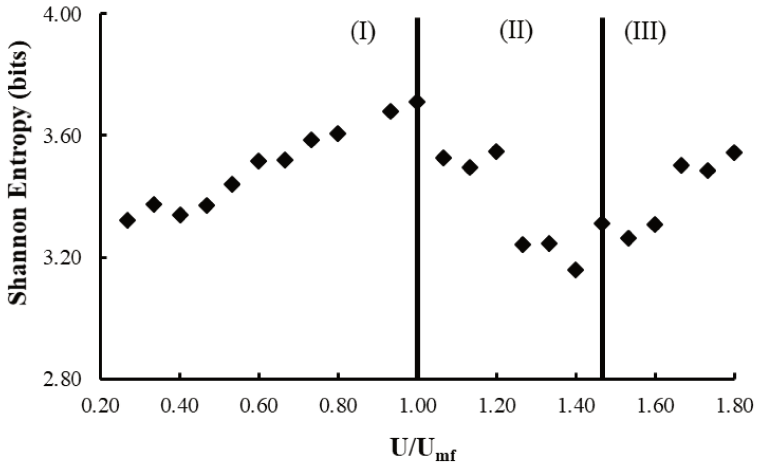

(b)

When U/U_{mf} < 1.00, that is, the expanded bed or particulate regime, the Shannon entropy increases with the superficial gas velocity. This is a reflection of the also increasing complexity and disorder of the gas-particle dynamics. In this region, the fluid begins only percolating the particles and then, the movement of the bed intensifies, altering the bed voidage, as the minimum fluidization point is approached. The Shannon entropy increases until it reaches maximum values around the minimum fluidization point. A possible explanation for this is that the preferential paths formed during the particulate regime disrupt, allowing the gas to pass through. Furthermore, in the vicinity of the minimum fluidization velocity, the fluctuations caused by the formation, coalescence and breaking of the bubbles inside the bed up to the surface is pointed as the responsible for the increase in the complexity of the system.

The slug flow regime gives the impression of a region distinguished by a lot of agitation and disorder. Counterintuitively, the Shannon entropies for this regime were actually lower than the minimum fluidization point. This effect is clearer for the B and D particles. The reason for that is the periodicity caused by the pulsation of the bed, characteristic of the slug flow regime. If a system starts to exhibit a periodic behavior, one can interpret that the system just became more ordered, in other words, less complex. Consequently, the reflection of this in the Shannon entropy analysis is a drop in this parameter.

Finally, the bubbling regime is the intermediate state between the minimum fluidization point and the slug flow regime. Generally, the values of the Shannon entropy for this region showed a negative slope, until it arrived at a minimum.

Table 4.7 is a comparison of the Shannon entropy at the minimum fluidization point among the three particles.

Table 4.7 – Comparison of the Shannon entropy at the minimum fluidization point.

Geldart classification	Particle load (kg)	Shannon entropy (bits)
A	0.4	3.75
	0.8	3.96
B	0.4	3.62
	0.8	3.66
D	0.4	3.54
	0.8	3.71

Higher values of entropy were observed for the case of 0.8 kg particle load. Wang et al. (2017) reasons that the Shannon entropy increases with the bed mass due to the increase of the fluctuation amplitude. This increase in the amplitude is translated in a large standard deviation and, by extension, a broader frequency distribution. Altering the shape of the distribution will also affect the value of the Shannon entropy. Additionally, the particle A were the ones who presented higher values of *H*. Prieto et al. (2017.b) found the same trend in the analysis of simulated pressure drop time series, obtained through computational fluid dynamics. The authors discusses that one possible explanation for this result is the size of the A particles. Because they have a smaller diameter than the others, the minimum fluidization is more vigorous, and by extension, more complex, while the B and D glass beads have a more discrete minimum fluidization and therefore less complex.

Alternatively, the frequency distributions can be modelled as probability density functions. Following the analysis of the minimum fluidization time series of 0.8 kg B glass beads, Table 4.8 is its result of the Kolmogorov-Smirnov test

Table 4.8 – Results of the Kolmogorov-Smirnov test (5% of significance and $D_c = 0.25907$) and the parameters of the PDF models for the minimum fluidization point of 0.8 kg B glass beads.

Distribution	***D***	**Sum of the quadratic errors (x10^3)**	**Parameters**
Normal	0.0536	1.49	$\mu = 865.90$ $\sigma = 14.15$
log-Normal	0.0569	1.53	$\mu = 6.76$ $\sigma = 0.02$
Logistic	0.0417	0.65	$\mu = 865.94$ $s = 8.65$
Gumbel	0.1059	3.51	$\alpha = 863.13$ $\beta = 12.89$
Weibull	0.0564	1.91	$\lambda = 868.84$ $k = 66.95$
Gamma	0.7731	83.7	$\theta = 60.12$ $k = 15.04$
Beta	0.6277	74.3	$\alpha = 2.92$ $\beta = 0.36$
Pearson III	0.6277	83.7	$\alpha = 5.16$ $\theta = 60.12$ $k = 15.04$
Exponential	1.0000	100	$\lambda = 1.00$
Maxwell	1.0000	100	$a = 15.00$
Rayleigh	1.0000	100	$a = 90.00$
Cauchy	0.9733	98.5	$\gamma = 863.93$
Chi-square	1.0000	100	$n = 2.00$

According to the Kolmogorov-Smirnov test, the Normal, log-Normal, Logisitic, Gumbel and Weibull distribution are a good fit for the experimental data. However, the Logistic

distribution presents the lowest value of the sum of the quadratic error, which, as mentioned previously, becomes the criterion for selecting the best fit if there are more than one probability density function approved in the K-S test. Figure 4.9 shows the fitting of the best PDF with the respective experimental frequency distribution.

Figure 4.9 – Frequency distribution of the minimum fluidization of 0.8 kg of B glass beads modelled as the Logistic distribution.

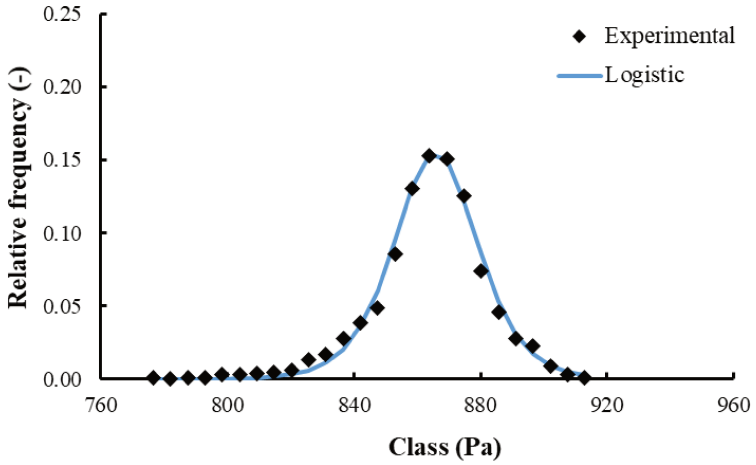

Tables A.1 to A.6 in Appendix A are the best fit of probability density functions for the fluidization of the A, B and D particles. The procedure was the same used in the election of the best PDF for the minimum fluidization point of 0.8 kg of B glass beads. Figure 4.10 is the fitting of the best PDF for frequency distributions of different fluidization regimes.

Figure 4.10 – Frequency distribution of the fluidization of 0.8 kg of B glass beads modelled as probability density functions – (a) $U/U_{mf} = 0.92$, (b) $U/U_{mf} = 2.45$ and (c) $U/U_{mf} = 4.34$.

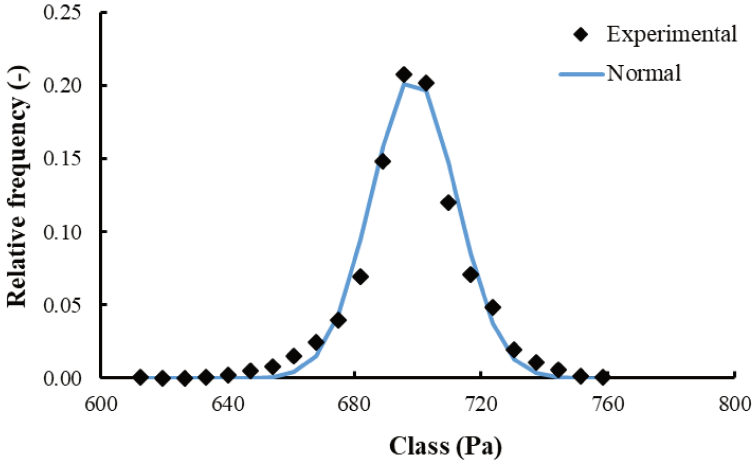

(a)

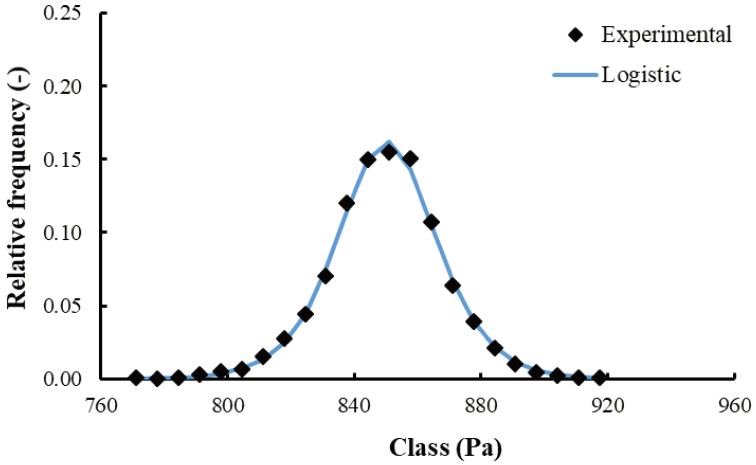

(b)

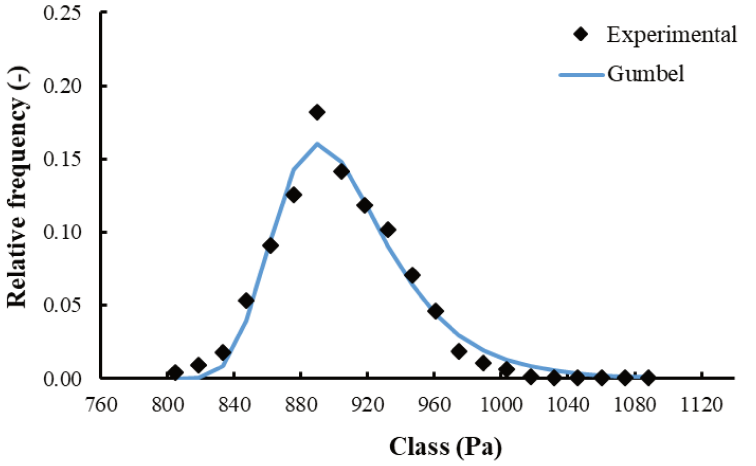

(c)

Figure 4.9 and Figure 4.10 show that the frequency distributions can be well represented by theoretical probability density functions, even when the distributions present long tails, that is, are asymmetric. Originally, Shannon (1948) defined the entropy for the discrete case. However, when this parameter is extended for the continuous case, it is called differential entropy, being readily calculated from the equations in Table 2.6. As it was mentioned in the theoretical foundation, the concept of average uncertainty carried by Shannon entropy it is not extended to its differential form. Instead, the differential entropy is understood as a function of the parameters of a distribution that describes how uncertainty changes as the parameters are modified. Nonetheless, the theoretical distribution functions can represent well the experimental frequency distributions, as it is showed in Figure 4.9 and Figure 4.10.

5. CONCLUSIONS

This dissertation evaluated the capacity of the Shannon entropy to characterize and identify fluidization regimes by analysing pressure drop time series from a gas-particle fluidized bed, varying the particle diameter and the total load in the bed.

The Shannon entropy comes from the information theory. This parameter is associated with the uncertainty of a random variable. In fluidization studies, it is linked with a kind of instability or complexity of the particulate system. This technique, likewise the method of moments, is relatively easily applied to a time series but it also has the advantage of giving physical meaning to the results instead of being just a statistical parameter. Yet, there are only few and recent studies on the Shannon entropy in particulate systems. The general trend was that Shannon entropy increased with the superficial gas velocity, with the highest values found in the region near the minimum fluidization point, and then it dropped slightly. An interesting comparison of results was made with the Kolmogorov entropy and correlation dimension, analysed by Prieto (2014). The chaotic invariants are related to the disorder, and by extension, the complexity of the system. The results are in agreement, that is, the point of minimum fluidization is usually where the highest values of the Shannon and Kolmogorov entropy were found. However, the periodic behavior of the slug flow regime caused a sudden drop in the latter parameter. It has to be taken into consideration that The Shannon entropy comes from a frequency distribution and the slug flow regime presented a large pressure drop variation, due to the pulsation of the bed that also caused the periodic behavior just mentioned. Hence, the stretched frequency distribution and probability density function, due to the large standard deviation, would be a difficulty for the Shannon to follow the Kolmogorov entropy profile. The chaotic invariants are evaluated in the state space, thus, the large standard deviation did not seem to prevent both the Kolmogorov entropy and the correlation dimension to capture this periodic and less complex behavior of the bed.

Moreover, the Shannon entropy analysis is only possible when the time series is transformed into a frequency distribution. Hence, the determination of the number of bins is a pertinent step in this analysis. The method of the coefficient of variation was used for this task, instead of conventional rules, such as the Sturges' and Scott's rule, due to the fact that it did not only depend on the total number of points in the time series nor it overestimated the number of classes. Once the frequency distribution was built, the Shannon entropy could be evaluated. Also, a theoretical probability density function could be used to fit the experimental data. The

shape of the frequency distribution influenced the best model to describe the data. For instance, when the distribution were symmetric, usually the Normal distribution was the PDF selected. Nonetheless, generally, the experimental frequency distributions exhibited a right or a left tail. The Logistic and Weibull distribution were the ones that usually presented the smallest quadratic error, suggesting that they are the most generic probability density functions to express the pressure fluctuations of the fluidization of A, B and D glass beads.

Lastly, this dissertation shows that the main premise of the pressure drop time series analysis is that the differences among them will result in some quantifiable parameter which would be able to characterize regimes. Because the interpretation of the data is not trivial, there are several techniques. The concept of which one of these methods is the best is relative. It ultimately depends on the objective of the analysis. For instance, if the objective is to construct the fluidization curve, the method of moments is enough. Moreover, the properties of the A, B and D particles have to be taken into consideration as they will fluidize differently. The B particles bubble at the minimum fluidization velocity while the D ones presented the formation of bubbles before that point. The A particles have a rapid transition between the particulate and slug flow regime. These characteristics had a reflect on the analysis. Therefore, even if the Shannon entropy presented some limitations or pitfalls, such as little sensitivity to the transition points, it could be used to auxiliate on the identification and characterization of fluidization regimes.

5.1 Recommendations for future work

Finally, here are some recommendations for future work:

- Evaluate the influence that different kinds of particles have in the time and frequency domain and the state space analysis. In order to do so, some parameters that could be studied are:
  - particle density;
  - particle diameter (different from the glass beads studied here);
  - sphericity;
  - bed diameter;
- evaluate the behavior of the time series in further fluidization states, such as the turbulent regime and the pneumatic transport;

- since the Laboratory of Processes in Porous Media (LPMP/FEQ/Unicamp) has optical fibers, previously used in a circulating fluidized bed, it would be interesting to measure simultaneously the pressure drop and the volumetric concentration of solids, comparing and complementing their analysis with themselves;
- evaluate other rigorous methods for the selection of the number of bins and attempt to improve the *CV* method. For instance, fit a polynomial or exponential curve to the *CV* versus *n* plot and calculate the derivative to determine the optimum number of class, instead of determining it visually, by the intersection of two straight lines that depict the trend of the curve;
- investigate deeper the differential entropy, and its properties that differs from the original discrete case, in the analysis of gas-particle fluidization regimes;
- lastly, it is proposed to take the analysis studied in this Dissertation beyond just characterizing fluidization states, but actually applying them in process control. For instance, to use parameters such as the Shannon entropy to control the optimal heat and mass transfer in a drying or reaction process in a fluidized bed or another multiphase system.

REFERENCES

ABRAMOWITZ, M.; STEGUN, I. A. *Handbook of Mathematical Functions with Formulas, Graphs, and Mathematical Tables*. 10th ed. New York: Dover, 1972.

BAE, K.; LIM, J. H.; KIM, J. H.; LEE, D. H.; HAN, J. H.; PARK, S. H.; LEE, D. H. Bubble characteristics by pressure fluctuation analysis in gas-solid bubbling fluidized beds with or without internal. *Korean Journal of Chemical Engineering*, v. 34, n. 2, p. 566-573, 2017.

BALTZER, H.; TATE, N. J.; KADUK, J.; HARPER, D.; PAGE, S.; MORRISON, R.; MUSKULUS, M.; JONES, P. Multi-Scale Entropy Analysis as a Method for Time-Series Analysis of Climate Data. *Climate*, v. 3, p. 227-240, 2015.

BEAL, M. J. *Variational Algorithms for Approximate Bayesian Inference*. 2003. 269 f. Tese (Doutorado em Física) – University College London, London. 2003.

BI, H. T.; ELLIS, N.; ABBA, I. A.; GRACE, J. R. A state-of-the-art review of gas-solid turbulent fluidization. *Chemical Engineering Science*, v. 55, p. 4789-4825, 2000.

BOHM, G.; ZECH, G. *Introduction to Statistics and Data Analysis for Physicists*. 1st ed. Hamburg: DESY, 2010.

BREAULT, R. W.; CASLETON, E. M., GUENTHER, C. P. Chaotic and statistical tests on fiber optic dynamic data taken from the riser section of a circulating fluidized bed. *Powder Technology*, v. 220, p. 151-163, 2012.

BRIENS, C.; McDOUGALL, S.; CHAN, E. On-line detection of bed fluidity in a fluidized bed coker. *Powder technology*, v. 138, p. 160-168, 2003.

BRIONGOS, J. V.; ARAGÓN, J. M.; PALANCAR, M. C. Fluidised bed dynamics diagnosis from measurements of low-frequency out-bed passive acoustic emissions. *Powder Technology*, v. 162, p. 145-156, 2006.

BROWN, R. C.; BRUE, E. Resolving dynamical features of fluidized beds from pressure fluctuations. *Powder Technology*, n. 119, p. 68-80, 2001.

BULUSU, K. V.; PLESNIAK, M. W. Shannon Entropy-Based Wavelet Transform Method for Autonomous Coherent Structure Identification in Fluid Flow Field Data. *Entropy*, v. 17, p. 6617-6642, 2015.

BURRUS, C. S.; GOPINATH, R. A.; GUO, H. *Introduction to wavelets and wavelet transforms: a primer*. 1st ed. New Jersey: Prentice-Hall, 1998.

BUTZGE, J. J. *Controle do regime fluidodinâmico estável durante o processo de umedecimento de inertes em leito de jorro utilizando análise espectral*. 2012. 127 f. Dissertação (Mestrado em Engenharia Química) – Faculdade de Engenharia Química, Universidade Estadual de Campinas, Campinas. 2012.

CAI, L.; JIAYING, C.; GUILING, X.; PAN, X.; XIAOPING, C.; CHANGSUI, Z. Experimental investigation and stability analysis on dense-phase pneumatic conveying of coal and biomass at high pressure. *Korean J. Chem. Eng.*, v. 30, n. 2, p. 295-305, 2013.

CASTILHO, G. J. *Determinação experimental das distribuições radial e axial de concentrações de sólidos em uma seção* riser *utilizando sonda de fibras ópticas*. 2007. 103 f. Dissertação (Mestrado em Engenharia Química) – Faculdade de Engenharia Química, Universidade Estadual de Campinas, Campinas. 2007.

CASTILHO, G. J. *Análise de caos em leito fluidizado circulante*. 2011. 164 f. Tese (Doutorado em Engenharia Química) – Faculdade de Engenharia Química, Universidade Estadual de Campinas, Campinas. 2011.

CHAPLIN, G.; PUGSLEY, T.; WINTERS, C. Application of chaos analysis to pressure fluctuation data from a fluidized bed dryer containing pharmaceutical granule. *Powder Technology*, v. 142, p. 110-120, 2004.

CHEN, X.; CHEN, D. Measuring Average Particle Size for Fluidized Bed Reactors by Employing Acoustic Emission Signals and Neural Networks. *Chemical Engineering Technology*, v. 31, p. 95-102, 2008.

CHEREMISINOFF, N. P. *Handbook of Chemical Processing Equipment*. 1st ed. Woburn: Butterworth-Heinemann, 2000.

CHONG, Y. O.; O'DEA, D. P.; WHITE, E. T.; LEE, P. L.; LEUNG, L. S. Control of the Quality of Fluidization in a Tall Bed Using the Variance of Pressure Fluctuations. *Powder Technology*, v. 53, p. 237-246, 1987.

CORREA, S. M. B. B. *Probabilidade e Estatística*. 2nd ed. Belo Horizonte: PUC Minas Virtual, 2003.

CREMASCO, M. A. *Operações unitárias em sistemas particulados e fluidomecânicos*. 2nd ed. São Paulo: Blucher, 2014.

CREMASCO, M. A.; PRIETO, W. H.; SCATENA, R.; MOURA, V. B. Study of spout zone of a conical spouted bed by Shannon entropy. In: XXXVIII Congresso Brasileiro de Sistemas Particulados, Maringá – PR, 2017. Anais do XXXVIII Congresso Brasileiro de Sistemas Particulados, 2017.

CROOKS, G. E. Field Guide to Continuous Probability Distributions. Disponível em: http://threeplusone.com/FieldGuide.pdf. Acesso em: 01 de ago. 2017.

DAVIES, C. E.; CARROLL, A.; FLEMMER, R. Particle size monitoring in a fluidized bed using pressure fluctuations. *Powder Technology*, v. 180, p. 307-311, 2008.

DAW, C. S.; LAWKINS, W. F.; DOWNING, D. J.; CLAPP JR., N. E. Chaotic characteristics of a complex gas-solids flow. Physical Review A, v. 41, n. 2, p. 1179-1181, 1990.

DE MARTÍN, L.; BRIONGOS, J. V.; ARAGÓN, J. M.; PALANCAR, M. C. Can low frequency accelerometry replace pressure measurements for monitoring gas-solid fluidized bed?. *Chemical Engineering Science*, v. 65, p. 4055-4064, 2010.

DUAN, F.; CONG, S. Shannon Entropy Analysis of Dynamic Behavior of Geldart Group B and Geldart Group D Particles in a Fluidized Bed. *Chemical Engineering Communications*, v. 200, n. 4, p. 575-586, 2013.

FAN, L. S.; ZHU, C. *Principles of Gas-Solid Flows*. 1st ed. Cambridge: Cambridge University Press, 1998.

FELIPE, C. A. S. Identificação e monitoramento de regime fluidodinâmico em leitos fluidizados gás-sólido. 2004. 209 f. Tese (Doutorado em Engenharia Química) – Faculdade de Engenharia Química, Universidade Estadual de Campinas, Campinas. 2004.

FELIPE, C. A. S.; ROCHA, S. C. S. Prediction of minimum fluidization velocity of gas-solid fluidized beds by pressure fluctuation measurements – Analysis of the standard deviation methodology. *Powder Technology*, v. 174, p. 104-113, 2007.

FERRARA, N. F.; PRADO, C. P. C. *Caos: uma introdução*. São Paulo: Blucher, 1994.

GELDART, D. Types of Gas Fluidization. *Powder Technology*, v. 7, p. 285-292, 1973.

GRACE, J. R. Contacting modes and behaviour classification of gas-solid and other two-phase suspensions. *The Canadian Journal of Chemical Engineering*, v. 64, n. 3, p. 353-363, 1986.

GREEN, D. W.; PERRY, R. H. *Perry's Chemical Engineers' Handbook*. 8th ed. New York: McGraw-Hill, 2008.

GUO, Q.; YUE, G.; WERTHER, J. Dynamics of Pressure Fluctuations in a Bubbling Fluidized Bed at High Temperature. *Ind. Eng. Chem. Res.*, v. 41, p. 3482-3488, 2002.

GYAN, R. *Time-series analysis of pressure fluctuation in gas-solid fluidized beds*. 2015. 96 f. Dissertação (Mestrado em Engenharia Química) – University of KwaZulu-Natal, Durban. 2015.

JAIBOON, O. A.; CHALERMSINSUWAN, B.; MEKASUT, L.; PIUMSOMBOON, P. Effect of flow pattern on power spectral density of pressure fluctuation in various fluidization regimes. *Powder Technology*, v. 233, p. 215-226, 2013.

JI, H.; OHARA, H.; KURAMOTO, K.; TSUTSUMI, A.; YOSHIDA, K.; HIRAMA, T. Nonlinear dynamics of a gas-solid circulating fluidized-bed system. *Chemical Engineering Science*, v. 55, p. 403-410, 2000

JOHNSSON, F.; ZIJERVELD, R. C.; SCHOUTEN, J. C.; VAN DEN BLEEK, C. M.; LECKNER, B. Characterization of fluidization regimes by time-series analysis of pressure fluctuations. *International Journal of Multiphase Flow*, v. 26, p. 663-715, 2000.

KAGE, H.; AGARI, M.; OGURA, H.; MATSUNO, Y. Frequency analysis of pressure fluctuation in fluidized bed plenum and its confidence limit for detection of various modes of fluidization. *Advanced Powder Technology*, v. 11, n. 4, p. 459-475, 2000.

KAI, T.; FURUSAKI, S. Methanation of carbon dioxide and fluidization quality in a fluid bed reactor – The influence of a decrease in gas volume. *Chemical Engineering Science*, v. 42, n. 2, p. 335-339, 1987.

KUNII, D.; LEVENSPIEL, O. *Fluidization Engineering*. 2nd ed. Stoneham: Butterworth-Heinemann, 1991.

LAZO, A. C. G. V.; RATHIE, P. N. On the Entropy of Continuous Probability Distributions. *IEEE Transactions on Information Theory*, v. 24, n. 1, p. 120-122, 1978.

LUCKOS, A.; COETZER, R.; MOSTERT, A. Description of Pressure Fluctuation in a Circulating Fluidized Bed by Statistical Analysis. In: 10th International Conference on Circulating Fluidized Beds and Fluidization Technology, Sun River, United States of America, 2011.

MICHALOWICZ, J. V.; NICHOLS, J. M.; BUCHOLTZ. *Handbook of Differential Entropy*. 1st ed. Boca Raton: CRC Press, 2013.

MONTEIRO, L. H. A. *Sistemas Dinâmicos*. 3rd ed. São Paulo: Editora Livraria da Física, 2011.

MORETTIN, P. A.; TOLOI, C. M. *Análise de Séries Temporais*. 2nd ed. São Paulo: Blucher, 2006.

MUN, J. *Advanced Analytical Models: Over 800 Models and 300 Applications from the Basel II Accord to Wall Street and Beyond*. 1st ed. Hoboken: Wiley Finance, 2008.

NECKEL, V. J. *Estatística I*. 1st ed. Joinville: Sociesc, 2016.

O'CONNOR, P. D. T.; KLEYNER, A. *Practical Reliability Engineering*. 5th ed. Chichester: John Wiley & Sons, 2012.

PRIETO, W. H. *Aplicação da teoria do caos em um leito fluidizado utilizando-se partículas A, B e D da classificação Geldart*. 2014. 127 f. Dissertação (Mestrado em Engenharia Química) – Faculdade de Engenharia Química, Universidade Estadual de Campinas, Campinas. 2014.

PRIETO, W.H.; MOURA, V. B.; SCATENA, R.; CREMASCO, M. A. Probabilistic study of minimum fluidization pressure time series for particles A, B & D of Geldart's classification. In: XXXVIII Congresso Brasileiro de Sistemas Particulados, Maringá – PR, 2017. Anais do XXXVIII Congresso Brasileiro de Sistemas Particulados, 2017.a.

PRIETO, W.H.; MOURA, V. B.; SCATENA, R.; CREMASCO, M. A. Theoretical application of Shannon's entropy in the analysis of the minimum fluidization conditions. In: XXXVIII Congresso Brasileiro de Sistemas Particulados, Maringá – PR, 2017. Anais do XXXVIII Congresso Brasileiro de Sistemas Particulados, 2017.b.

PUNCOCHAR, M.; DRAHOS, J. Origin of pressure fluctuations in fluidized bed. *Chemical Engineering Science*, v. 60, p. 1193-1197, 2005.

SANTAMARÍA-BONFIL, G.; FERNÁNDEZ, N.; GERSHENSON, C. Measuring the Complexity of Continuous Distributions. *Entropy*, v. 18, n. 3, p.1-18, 2016.

SASIC, S.; LECKNER, B.; JOHNSSON, F. Time-frequency investigation of different modes of bubble flow in a gas-solid fluidized bed. *Chemical Engineering Journal*, v. 121, p. 27-35, 2006.

SAXENA, S. C.; RAO, N. S.; TANJORE, V. N. Diagnostic Procedures for Establishing the Quality of Fluidization of Gas-Solid Systems. *Experimental Thermal and Fluid Science*, v. 6, p. 56-73, 1993.

SCOTT, D. W. On Optimal and Data-Based Histograms. *Biometrika*, v. 66, n. 3, p. 605-610, 1979.

SHANNON, C. E. A Mathematical Theory of Communication. T*he Bell System Technical Journal*, v. 27, 9. 379-423, 1948.

SILVA, C. A. M. *Aplicação de tecnologia analíticas de processo e inteligência artificial para monitoramento e controle de processo de recobrimento de partículas em leito fluidizado*. 2015. 301 f. Tese (Doutorado em Engenharia Química) – Faculdade de Engenharia Química, Universidade Estadual de Campinas, Campinas. 2015.

SPIEGEL, M. R.; STEPHENS, L. J. *Schaum's Outline of Theory and Problems of Statistics*. 4th ed. New York: McGraw-Hill, 2008.

STRINGER, J. Is a fluidized bed a chaotic dynamic system?. *Proceedings of the 10th International Conference on Fluidized Bed Combustion*, v. 1, p. 265-272, 1989.

STURGES, H. A. The Choice of a Class Interval. *Journal of the American Statistical Association*, v. 21, n. 153, p. 65-66, 1926.

TIPPET, L. H. C. *The Methods of Statistics*. 4th ed. New York: John Wiley & Sons, 1951.

TRNKA, O.; VESELY, V.; HARTMAN, M. Identification of the State of a Fluidized Bed by Pressure Fluctuations. *AIChE Journal*, v. 46, n. 3, p. 509-514, 2000.

VAN DEN BLEEK, C. M.; SCHOUTEN, J. C. Can deterministic chaos create order in fluidized-bed scale-up?. *Chemical Engineering Science*, v. 48, n. 13, p. 2367-2373, 1993.

VAN OMMEN, J. R.; KORTE, R. J.; VAN DEN BLEEK, C. M. Rapid detection of defluidization using the standard deviation of pressure fluctuations. *Chemical Engineering and Processing*, v. 43, p. 1329-1335, 2004.

VAN OMMEN, J. R.; SASIC, S.; VAN DER SCHAAF, J.; GHEORGHIU, S.; JOHNSSON, F.; COPPENS, M. O. Time-series analysis of pressure fluctuations in gas-solid fluidized beds – A review. *International Journal of Multiphase Flow*, v. 37, p. 403-428, 2011.

VANDER STAPPEN, M. L. M. *Chaotic hydrodynamics of fluidized beds*. 1996. 236 f. Tese (Doutorado em Engenharia Química) – Delft University of Technology, Delft. 1996.

WANG, J.; ZHONG, W.; ZHANG, H. Characterization of Flow Regimes in Fluidized Beds by Information Entropy Analysis of Pressure Fluctuations. *The Canadian Journal of Chemical Engineering*, v. 95, p. 578-588, 2017.

WILKINSON, D. Determination of Minimum Fluidization Velocity by Pressure Fluctuation Measurement. *The Canadian Journal of Chemical Engineering*, v. 73, p. 562-565, 1995.

WU, B.; KANTZAS, A.; BELLEHUMEUR, C. T.; HE, Z.; KRYUCHKOV, S. Multiresolution analysis of pressure fluctuations in a gas-solids fluidized bed: Application to glass beads and polyethylene powder systems. *Chemical Engineering Journal*, v. 131, p. 23-33, 2007.

YANG, T. Y.; LEU, L. P. Study of transition velocities from bubbling to turbulent fluidization by statistic and wavelet multi-resolution analysis on absolute pressure fluctuations. *Chemical Engineering Science*, v. 63, p. 1950-1970, 2008.

YATES, J. G. *Fundamentals of Fluidized-bed Chemical Processes*. 1st ed. Thetford: The Thetford Press, 1983.

ZARGHAMI, R.; MOSTOUFI, N.; SOTUDEH-GHAREBAGH, R. Nonlinear Characterization of pressure Fluctuations in Fluidized Beds. *Industrial & Engineering Chemistry Research*, v. 47, p. 9497-9507, 2008.

ZHONG, W.; ZHANG, M. Characterization of dynamic behavior of a spout-fluid bed with Shannon entropy analysis. *Powder Technology*, v. 159, p. 121-126, 2005.

ZHONG, W.; JIN, B.; ZHANG, Y.; WANG, X.; ZHANG, M.; XIAO, R. Description of Dynamic Behavior of a Fluidized Bed with Biomass Fuels by Shannon Entropy Increment Analysis. *Energy & Fuels*, v. 23, p. 3167-3171, 2009.

ZIAEI-HALIMEJANI, H.; ZARGHAMI, R.; MOSTOUFI, N. Investigation of hydrodynamics of gas-solid fluidized beds using cross recurrence quantification analysis. *Advanced Powder Technology*, v. 28, p. 1237-1248, 2017.

APPENDIX A

Tables A.1 to A.6 are the best fit of probability density functions for each frequency distribution of the three types of particle.

Table A.1 – Best fit of probability density functions for the fluidization of 0.4 kg A glass beads.

U/U_{mf}	**Sum of the quadratic errors (x10^3)**	**Distribution**	**Parameters**
0.4348	7.60	Logistic	μ = 52.43 s = 0.50
0.4565	7.12	Logistic	μ = 63.29 s = 0.37
0.4783	2.50	Logistic	μ = 81.12 s = 0.70
0.5000	1.79	Logistic	μ = 101.27 s = 0.67
0.5217	8.04	Weibull	λ = 117.09 k = 195.90
0.5435	10.40	Gumbel	α = 131.93 β = 0.96
0.5652	6.68	Logistic	μ = 141.16 s = 0.45
0.5870	16.36	Weibull	λ = 158.90 k = 176.78
0.6087	4.79	Normal	μ = 166.26 σ = 1.38
0.6304	10.14	Weibull	λ = 205.67 k = 260.54
0.6522	4.99	Weibull	λ = 214.25 k = 176.53
0.6739	2.57	Normal	μ = 234.80 σ = 1.20

Table continued

U/U_{mf}	Sum of the quadratic errors (x10^3)	Distribution	Parameters
0.6957	13.74	Normal	μ = 243.90 σ = 1.37
0.7174	4.92	Gumbel	α = 290.16 β = 0.97
0.7391	1.88	Weibull	λ = 285.66 k = 180.09
0.7609	3.39	Gumbel	α = 307.76 β = 3.32
0.7826	2.15	Weibull	λ = 371.26 k = 379.95
0.8043	1.67	Logistic	μ = 382.83 s = 0.54
0.8261	8.74	Gumbel	α = 410.53 β = 1.60
0.8478	4.76	Logistic	μ = 449.32 s = 0.59
0.8696	6.52	Weibull	λ = 472.06 k = 422.32
0.8913	11.83	Gumbel	α = 472.86 β = 1.26
0.9130	1.54	Logistic	μ = 511.28 s = 1.09
0.9348	2.82	Weibull	λ = 556.18 k = 762.20
0.9565	4.10	Weibull	λ = 563.59 k = 667.35
0.9783	0.86	Normal	μ = 578.49 σ = 0.99
1.0000	0.71	Logistic	μ = 602.55 s = 0.52

Table continued

U/U_{mf}	Sum of the quadratic errors (x10^3)	Distribution	Parameters
1.0217	1.26	Logistic	μ = 604.39 s = 0.50
1.0652	13.54	Logistic	μ = 610.41 s = 3.17
1.0870	0.48	Logistic	μ = 609.57 s = 1.05
1.1087	0.66	Logistic	μ = 611.70 s = 0.92
1.1304	1.11	Normal	μ = 613.51 σ = 2.45
1.1522	0.79	Normal	μ = 615.37 σ = 2.18
1.1739	1.38	Normal	μ = 618.16 σ = 2.31
1.1957	1.91	Logistic	μ = 621.18 s = 1.24
1.2174	1.95	Weibull	λ = 624.94 k = 310.62
1.2391	1.56	Logistic	μ = 626.84 s = 1.02
1.2609	5.34	Normal	μ = 630.12 σ = 2.93
1.2826	0.86	Normal	μ = 633.09 σ = 2.47
1.3043	1.35	Logistic	μ = 636.10 s = 1.72

Table A.2 – Best fit of probability density functions for the fluidization of 0.8 kg A glass beads.

U/U_{mf}	**Sum of the quadratic errors (x10^3)**	**Distribution**	**Parameters**
0.4167	6.33	Logistic	μ = 52.84 s = 0.38
0.4375	4.67	Gumbel	α = 63.26 β = 1.19
0.4583	9.10	Weibull	λ = 81.37 k = 135.68
0.4792	6.23	Weibull	λ = 101.78 k = 178.98
0.5000	3.77	Weibull	λ = 117.12 k = 123.22
0.5208	1.91	Weibull	λ = 134.37 k = 121.84
0.5417	1.85	Logistic	μ = 139.47 s = 0.67
0.5625	6.52	Weibull	λ = 156.34 k = 281.70
0.5833	1.18	Weibull	λ = 165.85 k = 141.06
0.6042	4.58	Logistic	μ = 203.58 s = 0.63
0.6250	3.65	Normal	μ = 214.20 σ = 1.14
0.6458	3.58	Logistic	μ = 234.45 s = 0.48
0.6875	11.29	Gumbel	α = 281.29 β = 1.22
0.7292	5.44	Gumbel	α = 311.52 β = 2.94

Table continued

U/U_{mf}	Sum of the quadratic errors (x10^3)	Distribution	Parameters
0.7500	3.32	Weibull	λ = 374.16 k = 362.40
0.7708	1.30	Normal	μ = 387.38 σ = 1.46
0.7917	8.35	Normal	μ = 412.39 σ = 1.61
0.8125	10.78	Normal	μ = 455.24 σ = 1.99
0.8333	5.14	Logistic	μ = 484.27 s = 0.54
0.8542	4.81	Gumbel	α = 499.48 β = 1.51
0.8750	1.95	Logistic	μ = 547.15 s = 0.64
0.8958	0.39	Logistic	μ = 614.67 s = 0.75
0.9167	7.44	Normal	μ = 630.94 σ = 1.02
0.9375	7.01	Gumbel	α = 665.07 β = 1.80
0.9583	1.20	Gumbel	α = 719.33 β = 1.36
0.9792	1.85	Weibull	λ = 755.54 k = 634.65
1.0000	0.47	Logistic	μ = 773.33 s = 0.76
1.0208	8.47	Weibull	λ = 764.37 k = 84.11
1.0417	1.71	Gumbel	α = 761.04 β = 1.68

Table continued

U/U_{mf}	**Sum of the quadratic errors (x10^3)**	**Distribution**	**Parameters**
1.0625	3.33	Gumbel	α = 762.83 β = 2.40
1.0833	1.66	Gumbel	α = 765.62 β = 2.51
1.1042	1.29	Gumbel	α = 768.54 β = 1.69
1.1250	0.24	Logistic	μ = 771.44 s = 1.51
1.1458	1.62	Logistic	μ = 773.99 s = 1.67
1.1667	0.79	Logistic	μ = 775.97 s = 1.89
1.1875	0.51	Normal	μ = 778.53 σ = 3.45
1.2083	1.41	Normal	μ = 780.95 σ = 3.49

Table A.3 – Best fit of probability density functions for the fluidization of 0.4 kg B glass beads.

U/U_{mf}	**Sum of the quadratic errors (x10^3)**	**Distribution**	**Parameters**
0.6327	4.30	Logistic	μ = 157.18 s = 5.81
0.7143	8.01	Weibull	λ = 185.54 k = 20.52
0.7959	3.20	Weibull	λ = 255.85 k = 17.42
0.8367	4.56	Weibull	λ = 285.04 k = 19.23
0.8776	2.91	Normal	μ = 370.54 σ = 17.56
0.9184	1.58	Logistic	μ = 404.89 s = 10.90
0.9592	0.63	Logistic	μ = 458.25 s = 12.05
1.0000	1.59	Logistic	μ = 487.92 s = 12.35
1.0408	0.87	Logistic	μ = 485.52 s = 12.99
1.1633	0.88	Logistic	μ = 478.44 s = 14.18
1.3265	0.16	Logistic	μ = 471.99 s = 14.08
1.4286	0.78	Logistic	μ = 463.72 s = 14.24
1.5306	0.29	Logistic	μ = 458.63 s = 13.58
1.6327	0.26	Logistic	μ = 457.59 s = 14.03

Table continued

U/U_{mf}	Sum of the quadratic errors (x10^3)	Distribution	Parameters
1.7347	2.62	Logistic	μ = 459.60 s = 10.92
1.9388	2.23	Normal	μ = 463.43 σ = 22.77
2.0408	1.48	Weibull	λ = 471.86 k = 25.20
2.2449	0.64	Weibull	λ = 478.89 k = 23.34
2.4490	2.24	Weibull	λ = 481.99 k = 26.67
2.6531	3.01	Logistic	μ = 479.58 s = 10.79
2.8571	1.91	Logistic	μ = 481.63 s = 11.98
3.0612	2.60	Weibull	λ = 486.73 k = 29.03
3.4694	0.64	Logistic	μ = 487.04 s = 13.23
3.8776	0.69	Weibull	λ = 505.51 k = 21.62
4.2857	1.37	Logistic	μ = 512.46 s = 15.48
4.6939	1.94	Logistic	μ = 527.16 s = 18.05
5.1020	1.11	Normal	μ = 539.14 σ = 34.99
5.3061	0.50	Logistic	μ = 556.26 s = 17.96

Table A.4 – Best fit of probability density functions for the fluidization of 0.8 kg B glass beads.

U/U_{mf}	Sum of the quadratic errors (x10^3)	Distribution	Parameters
0.5472	2.58	Logistic	μ = 154.21 s = 7.20
0.5849	1.82	Logistic	μ = 173.62 s = 7.82
0.6226	1.22	Logistic	μ = 173.00 s = 8.42
0.6604	1.26	Weibull	λ = 259.12 k = 18.38
0.6981	0.84	Logistic	μ = 327.28 s = 8.56
0.7358	0.57	Normal	μ = 390.33 σ = 14.08
0.7736	2.51	Normal	μ = 425.96 σ = 11.39
0.8113	0.74	Logistic	μ = 515.40 s = 7.13
0.8491	1.34	Normal	μ = 562.07 σ = 12.51
0.8868	0.67	Logistic	μ = 636.76 s = 8.21
0.9245	2.33	Normal	μ = 698.75 σ = 13.30
0.9623	0.92	Normal	μ = 762.79 σ = 13.74
1.0000	0.65	Logistic	μ = 865.94 s = 8.65
1.0377	0.20	Logistic	μ = 8.6695 s = 8.59

Table continued

U/U_{mf}	Sum of the quadratic errors (x10^3)	Distribution	Parameters
1.0755	0.53	Normal	μ = 866.78 σ = 15.51
1.1132	0.61	Logistic	μ = 864.92 s = 8.53
1.1509	1.27	Normal	μ = 860.48 σ = 14.59
1.1887	1.75	Normal	μ = 854.03 σ = 13.34
1.2264	1.75	Normal	μ = 854.03 σ = 13.34
1.3208	0.14	Logistic	μ = 837.93 s = 9.43
1.4151	0.17	Logistic	μ = 833.76 s = 10.23
1.5094	0.52	Logistic	μ = 832.19 s = 9.11
1.6038	0.46	Normal	μ = 831.52 σ = 16.46
1.6981	3.44	Weibull	λ = 835.85 k = 95.01
1.7925	2.81	Normal	μ = 837.38 σ = 10.74
1.8868	0.78	Logistic	μ = 839.92 s = 10.22
2.0755	1.03	Normal	μ = 804.29 σ = 15.23
2.2642	0.38	Logistic	μ = 848.09 s = 10.33
2.4528	0.20	Logistic	μ = 850.30 s = 10.12

Table continued

U/U_{mf}	Sum of the quadratic errors (x10^3)	Distribution	Parameters
2.6415	0.45	Normal	μ = 852.20 σ = 20.62
2.8302	0.34	Normal	μ = 856.05 σ = 20.63
3.2075	0.66	Normal	μ = 860.64 σ = 23.37
3.5849	0.51	Normal	μ = 869.32 σ = 34.40
3.9623	0.85	Gumbel	α = 872.86 β = 32.37
4.3396	1.66	Gumbel	α = 898.87 β = 35.65
4.7170	1.37	Normal	μ = 920.94 σ = 31.01
4.9057	0.69	Normal	μ = 932.38 σ = 33.39

Table A.5 – Best fit of probability density functions for the fluidization of 0.4 kg D glass beads.

U/U_{mf}	Sum of the quadratic errors (x10^3)	Distribution	Parameters
0.4167	2.72	Weibull	λ = 364.23 k = 16.12
0.5000	1.64	Weibull	λ = 565.87 k = 25.53
0.5833	0.86	Weibull	λ = 803.42 k = 34.52
0.6667	0.69	Logistic	μ = 1,051.67 s = 15.13
0.7500	5.41	Weibull	λ = 1,392.56 k = 86.43
0.8333	4.85	Weibull	λ = 1,648.43 k = 104.59
0.9167	3.24	Weibull	λ = 2,032.45 k = 120.80
1.0000	2.59	Weibull	λ = 2,385.12 k = 127.87
1.1667	0.60	Weibull	λ = 2,359.26 k = 93.66
1.2500	3.04	Logistic	μ = 2,391.41 s = 12.90
1.3333	4.54	Weibull	λ = 2,441.95 k = 137.19
1.4167	3.91	Weibull	λ = 2,506.91 k = 138.01
1.5000	6.88	Weibull	λ = 2,492.48 k = 143.64
1.5833	3.90	Gumbel	α = 2,423.80 β = 24.86

Table continued

U/U_{mf}	**Sum of the quadratic errors (x10^3)**	**Distribution**	**Parameters**
1.6667	0.73	Logistic	μ = 2,494.45 s = 17.90
1.7500	0.80	Weibull	λ = 2,538.18 k = 94.63
1.8333	5.08	Weibull	λ = 2,536.72 k = 157.11
1.9167	11.59	Weibull	λ = 2,603.68 k = 173.01
2.0000	6.34	Logistic	μ = 2,701.26 s = 8.82
2.0833	3.65	Weibull	λ = 2,752.52 k = 179.36
2.1667	1.34	Weibull	λ = 2,906.61 k = 106.59

Table A.6 – Best fit of probability density functions for the fluidization of 0.8 kg D glass beads.

U/U_{mf}	Sum of the quadratic errors (x10^3)	Distribution	Parameters
0.2667	4.16	Logistic	μ = 427.74 s = 11.57
0.3333	2.78	Weibull	λ = 601.94 k = 28.98
0.4000	0.57	Logistic	μ = 802.34 s = 15.13
0.4667	0.29	Logistic	μ = 1,056.91 s = 16.52
0.5333	0.22	Logistic	μ = 1,331.89 s = 15.86
0.6000	2.48	Weibull	λ = 1,679.37 k = 93.25
0.6667	1.40	Weibull	λ = 1,988.72 k = 94.35
0.7333	2.36	Weibull	λ = 2,424.75 k = 127.33
0.8000	2.52	Weibull	λ = 2,809.95 k = 139.67
0.9333	1.31	Logistic	μ = 3,160.70 s = 16.33
1.0000	1.39	Weibull	λ = 3,375.72 k = 125.87
1.0667	2.79	Weibull	λ = 3,320.76 k = 176.51
1.1333	3.83	Weibull	λ = 3,367.99 k = 184.13
1.2000	2.82	Logistic	μ = 3,365.43 s = 14.20

Table continued

U/U_{mf}	Sum of the quadratic errors (x10^3)	Distribution	Parameters
1.2667	4.43	Logistic	μ = 3,353.88 s = 10.13
1.3333	2.96	Logistic	μ = 3,360.74 s = 13.23
1.4000	14.90	Gumbel	α = 3,390.39 β = 24.75
1.4667	0.75	Normal	μ = 3,429.28 σ = 31.02
1.5333	2.78	Normal	μ = 3,467.88 σ = 27.06
1.6000	1.14	Logistic	μ = 3,491.51 s = 16.69
1.6667	0.68	Logistic	μ = 3,527.89 s = 17.48
1.7333	0.29	Logistic	μ = 3,667.63 s = 18.70
1.8000	0.92	Weibull	λ = 3,789.60 k = 151.48